[redacted] UMRL 048

UNIVERSITY OF MICHIGAN

2541-1-F = RL-2058 2541-1-F 64 4 DEC 12

THE RADAR CROSS-SECTION OF THE B-57 AIRCRAFT AT X- AND S-BANDS

by

J. W. Crispin and T. B. Curtz

1971
1972
1973
6 1974
DEC 17 1974

Work performed for
the
CORNELL AERONAUTICAL LABORATORY, INC.,
Buffalo, New York

On C.A.L. Subcontract No. S-56-80
under Contract AF 18(600)-1550

27 June 1956

EXCLUDED FROM GDS
(DD FORM 254 GP-____)

"NATIONAL SECURITY INFORMATION
"Unauthorized Disclosure Subject to Crimi
Sanctions".

APPROVED BY Keeve M. Siegel
Keeve M. Siegel, Project Supervisor

DOWNGRADED AT 12 YEAR INTERVALS; NOT AUTOMATICALLY DECLASSIFIED. DOD DIR 5200.10

This document contains information affecting the national defense of the United States within the meaning of the Espionage Laws, Title 18, U.S.C., Sections 793 and 794. Its transmission or the revelation of its contents in any manner to an unauthorized person is prohibited by law.

UNCLASSIFIED

[redacted]

MISSING
PAGE

TABLE OF CONTENTS

LIST OF FIGURES

LIST OF FIGURES (Cont'd)

LIST OF TABLES

I

INTRODUCTION

The Cornell Aeronautical Laboratory, Inc. (C.A.L.) contracted with The University of Michigan to determine theoretically the monostatic radar cross-section of the B-57 Aircraft. These computations were begun on 7 May 1956 and were performed under C.A.L. subcontract No. S-56-80 under C.A.L. prime contract No. AF 18(600)-1550.

The problem involved the determination of the cross-section of the B-57 aircraft at X- and S-bands for horizontal and vertical polarization as a function of the azimuth angle for eight different elevation angles; the elevation angles ranged from 15 degrees above the horizontal to 90 degrees below the horizontal in 15-degree increments. The coordinate system used for these computations is shown in Figures 1-1 (a, b, and c) and 1-2. The first three of these figures show the orientation of the rectangular coordinate system with respect to the aircraft, and Figure 1-2 defines the polar angles β and γ used to denote elevation and azimuth, respectively.

To determine theoretically the cross-section of a complex shape such as an aircraft we carry out a series of three steps. The first step, necessary for economic reasons because of the extreme complexity of the mathematical expression for the shape of the aircraft, is to select proper combinations of simple shapes for the purpose of computing the cross-section of the aircraft itself. The second step is to determine the cross-sections of these parts. Here it is necessary to approximate the cross-sections for the simple shapes when their results are not known exactly. The third step is to combine the cross-sections

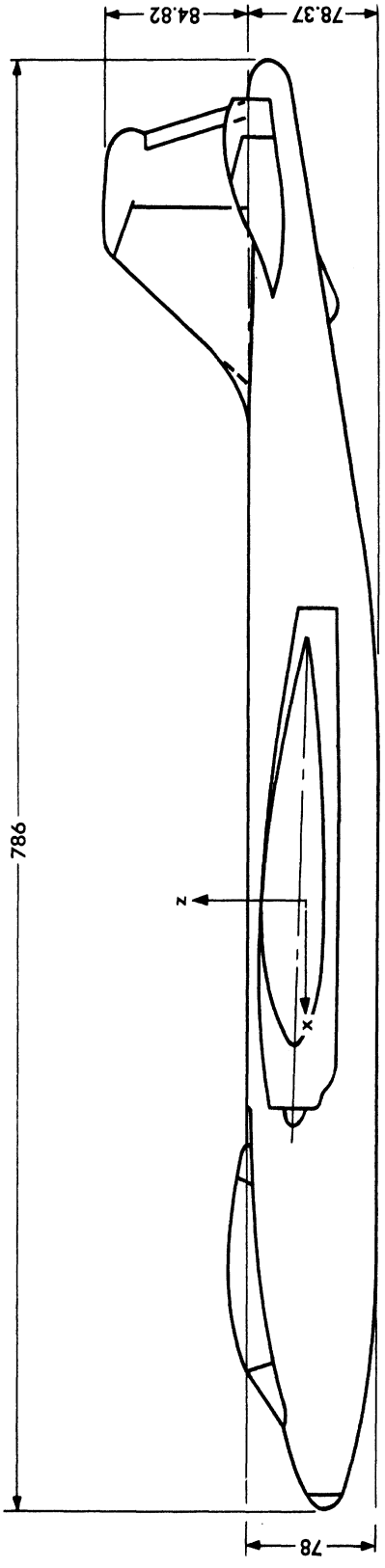

FIG. 1-1a SIDE VIEW OF THE B-57 SHOWING COORDINATE SYSTEM USED IN THE COMPUTATIONS (All Dimensions Shown Are in Inches)

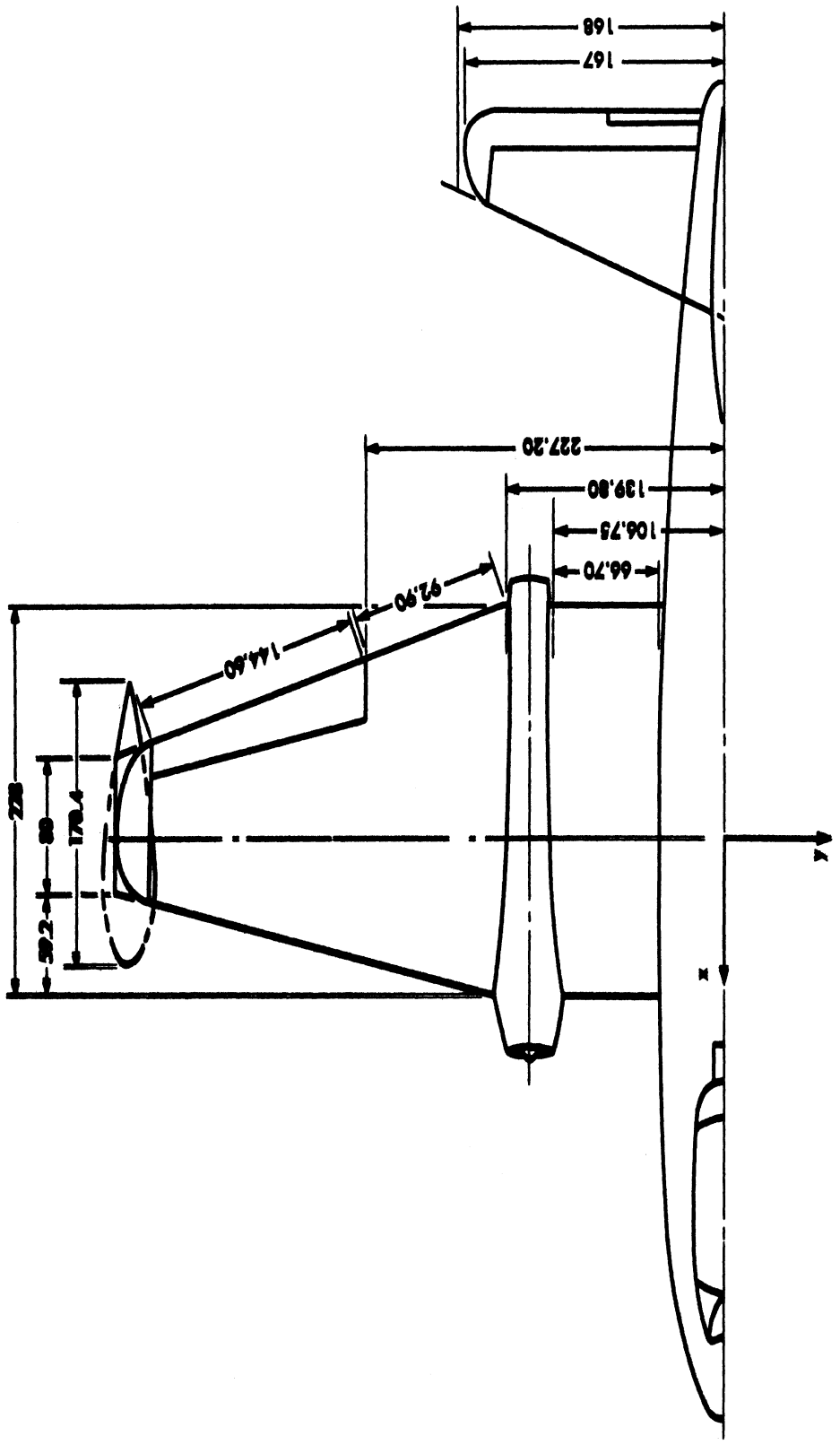

FIG. 1-1b TOP VIEW OF THE B-57 SHOWING COORDINATE SYSTEM USED IN THE COMPUTATIONS (All Dimensions Shown Are in Inches)

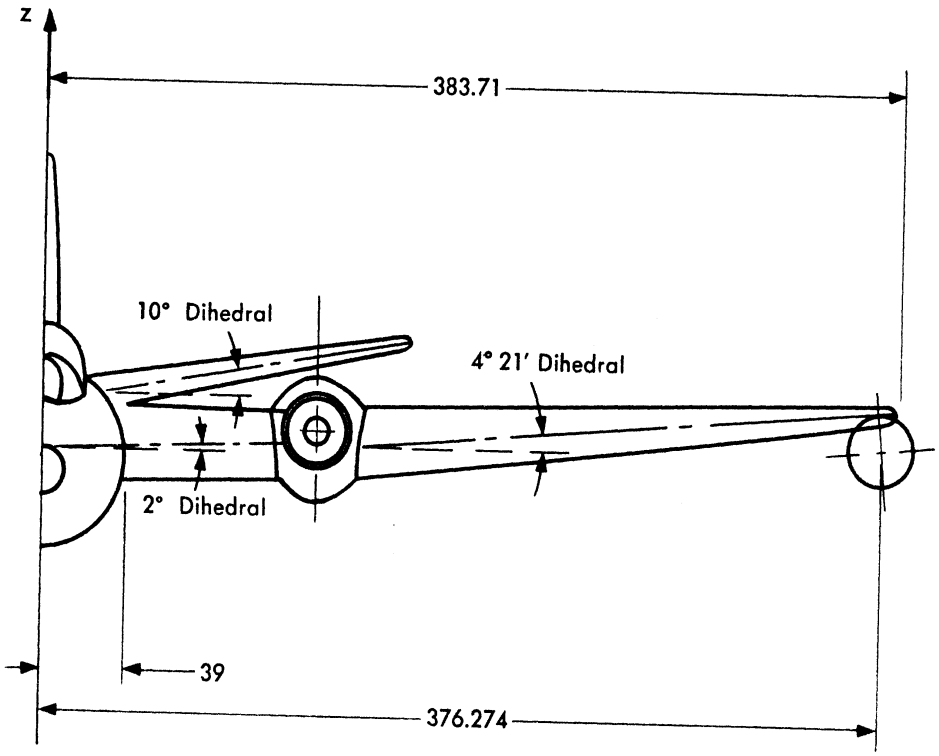

FIG. 1-1c FRONT VIEW OF THE B-57 SHOWING COORDINATE SYSTEM USED IN THE COMPUTATIONS (All Dimensions Shown Are in Inches)

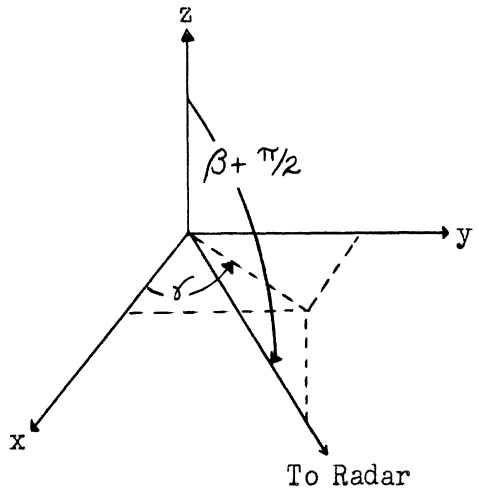

FIG. 1-2 COORDINATE SYSTEM (Defining the Aspect Angles β and γ)

of the parts of the aircraft, computed with the simple-shape approximations, in some appropriate manner so as to give the cross-section of the entire structure.

These three steps and their application are discussed in detail in Reference 1. The details of the application of the first two steps to the problem of determining the cross-section of the B-57 are given in Appendix A. The application of the third step is discussed in Appendix B. The results of the computations are presented in Section II.

II

THEORETICAL CROSS-SECTIONS AT X- AND S- BANDS

The theoretical monostatic radar cross-sections, $\sigma(\beta, \gamma)$, for the B-57 are presented in this section for X-band ($\lambda = 3$cm) and for S-band ($\lambda = 10$cm). Both horizontal and vertical polarizations are considered. From Figure 1-2 it is seen that the unit vector, $\hat{r}$, defining the direction from the radar to the origin of the coordinate system is given by

$$\hat{r} = (-\cos\beta\cos\gamma)\,\hat{i}_x + (-\cos\beta\sin\gamma)\,\hat{i}_y + (\sin\beta)\,\hat{i}_z \ .$$

Thus, we can define horizontal polarization to be the case for which the electric vector has the direction

$$\hat{p}_h = (-\sin\gamma)\,\hat{i}_x + (\cos\gamma)\,\hat{i}_y, \text{ for } \beta < 90^\circ; \text{ and}$$
$$\hat{p}_h = -\hat{i}_x, \text{ for } \beta = 90^\circ.$$

This results in vertical polarization being given by

$$\hat{p}_v = (\sin\beta\cos\gamma)\,\hat{i}_x + (\sin\beta\sin\gamma)\,\hat{i}_y + (\cos\beta)\,\hat{i}_z,$$
$$\text{for } \beta < 90^\circ; \text{ and}$$
$$\hat{p}_v = \hat{i}_y, \text{ for } \beta = 90^\circ.$$

The computational procedures used are given in detail in Appendices A and B; the results are presented in graphical form in Figures 2-1 through 2-14. Each figure displays $\sigma(\beta, \gamma)$ as a function of γ for a fixed value of the elevation angle, β. Both polarizations are included in each figure. Since for $\beta = 90^\circ$ the cross-section is independent of γ, a graphical display of the computational results is not required. Thus, the $\beta = 90^\circ$ results are presented

in Table 2.1. Table 2.1 also contains the values of the cross-section at other aspects near $\beta = 90^\circ$ to illustrate the pattern to be expected in the vicinity of $\beta = 90^\circ$.

The cross-section was computed for each value of β ($\beta = -15^\circ(15^\circ)75^\circ$) for $\gamma = 0^\circ(10^\circ)180^\circ$, and for those values of γ at which sharp peaks in the cross-section occur. These peaks are very sharp (in γ), and in the graphs we have shown upper bounds for the peak widths (Appendix B.3).

The radome located at the nose of the fuselage of the B-57 was assumed to be completely transparent and the interior of the hole was assumed to reflect the incident energy in an essentially isotropic fashion (see Appendix A).

Many of the angles involved in determining the cross-sections for the B-57 had to be measured with a protractor, and since some of the approximation formulas used are very sensitive to changes in the angle parameters, a slight difference in the measurement of an angle on an aircraft drawing can result in marked differences in the computed value of cross-section for a particular choice of β, γ, and λ. This fact should be kept in mind in examining Figures 2-1 through 2-14 and Table 2.1, especially in the vicinity of the sharp peaks.

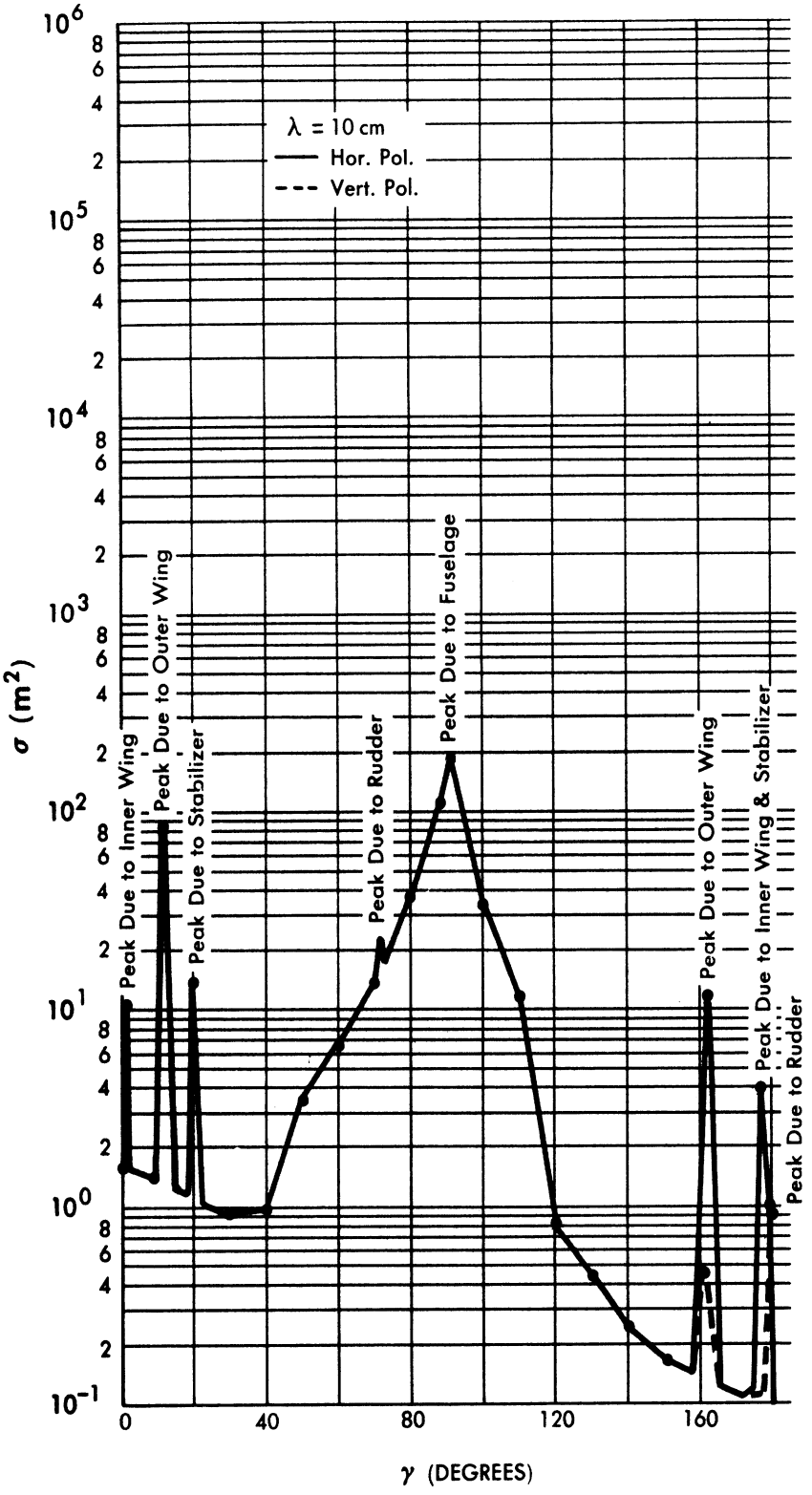

FIG. 2-1 RADAR CROSS-SECTION OF THE B-57 AT S-BAND FOR $\beta = -15°$

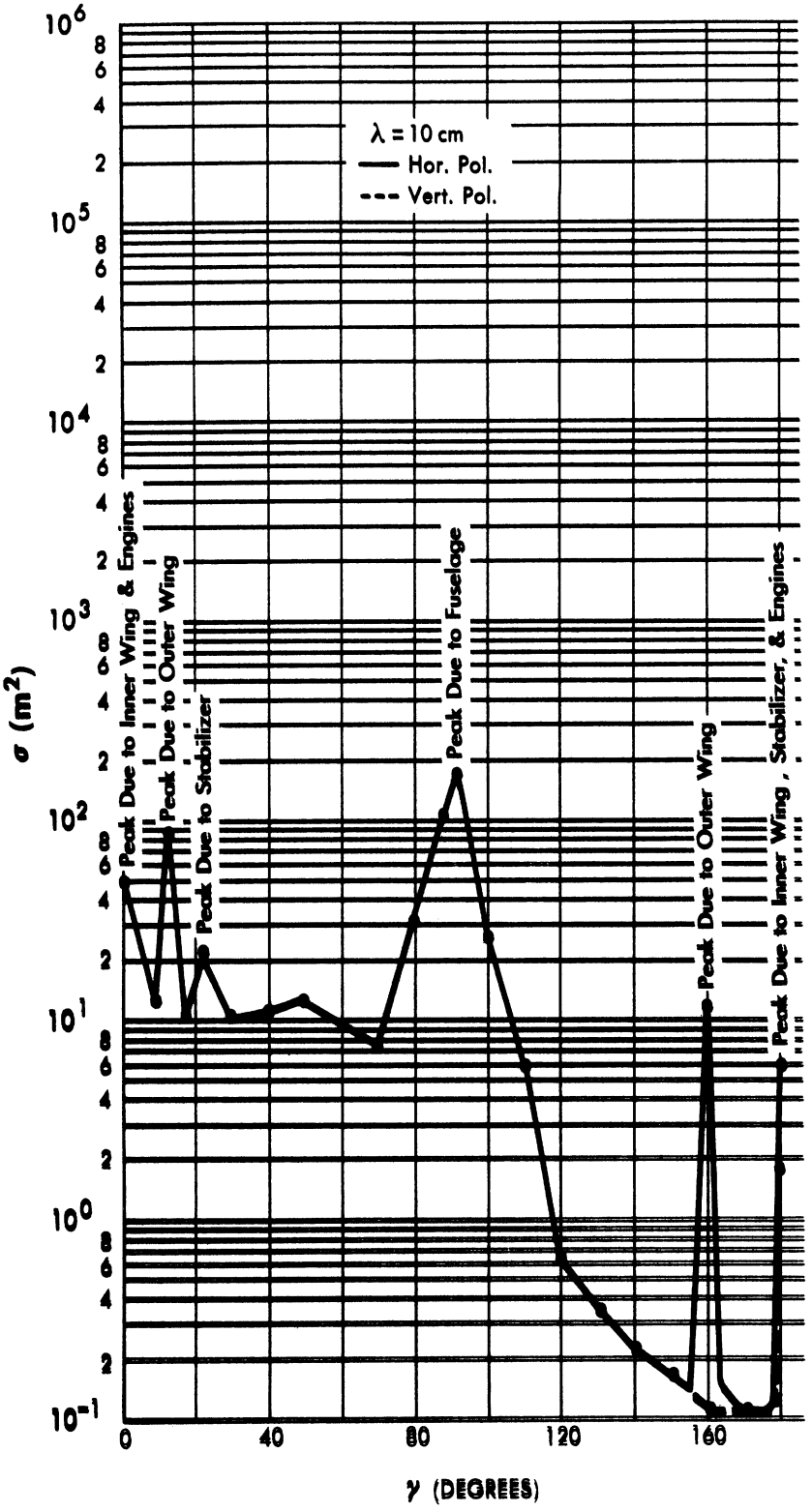

FIG. 2-2 RADAR CROSS-SECTION OF THE B-57 AT S-BAND FOR $\beta = 0°$

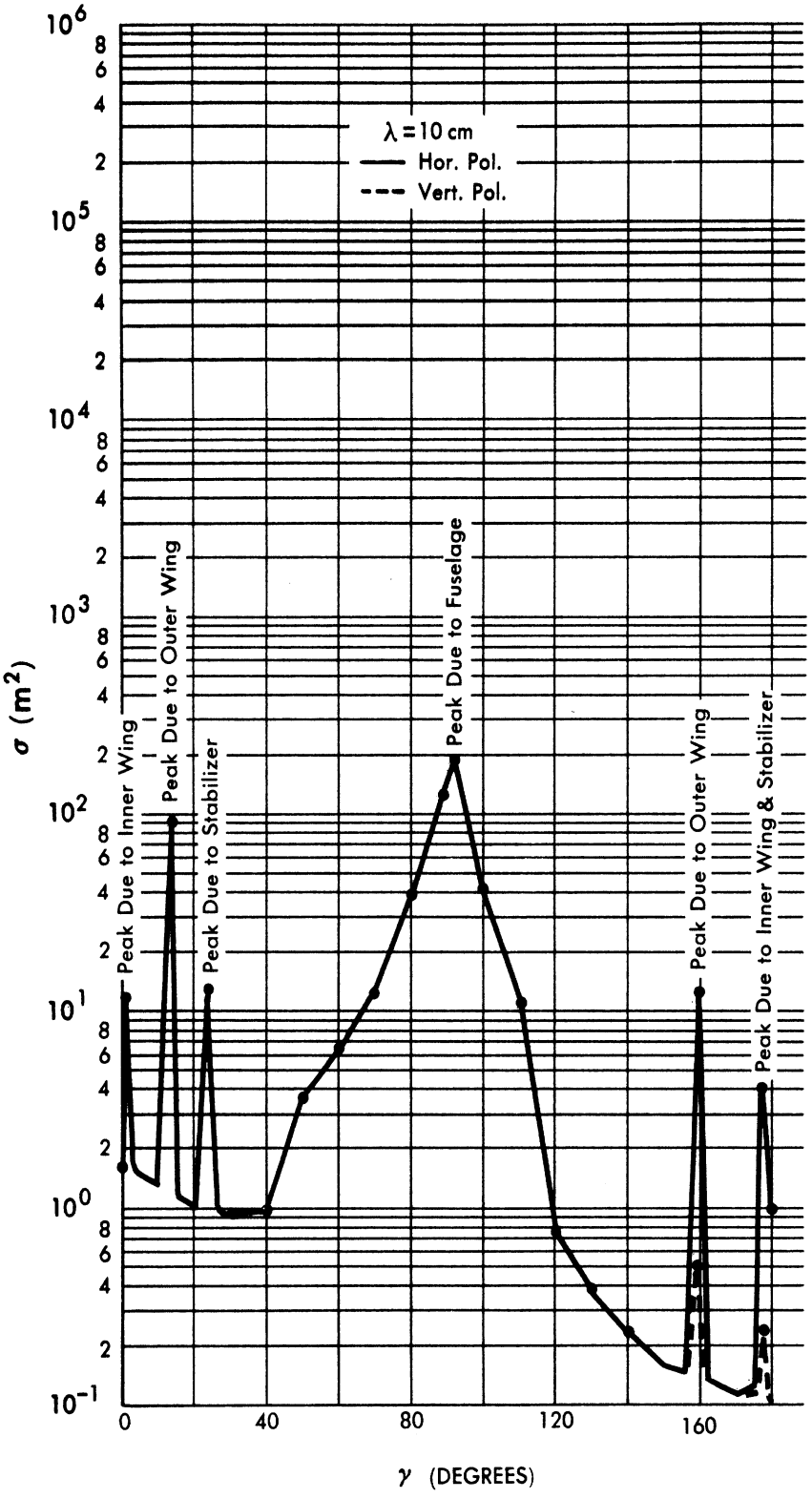

FIG. 2-3 RADAR CROSS-SECTION OF THE B-57 AT S-BAND FOR $\beta = 15°$

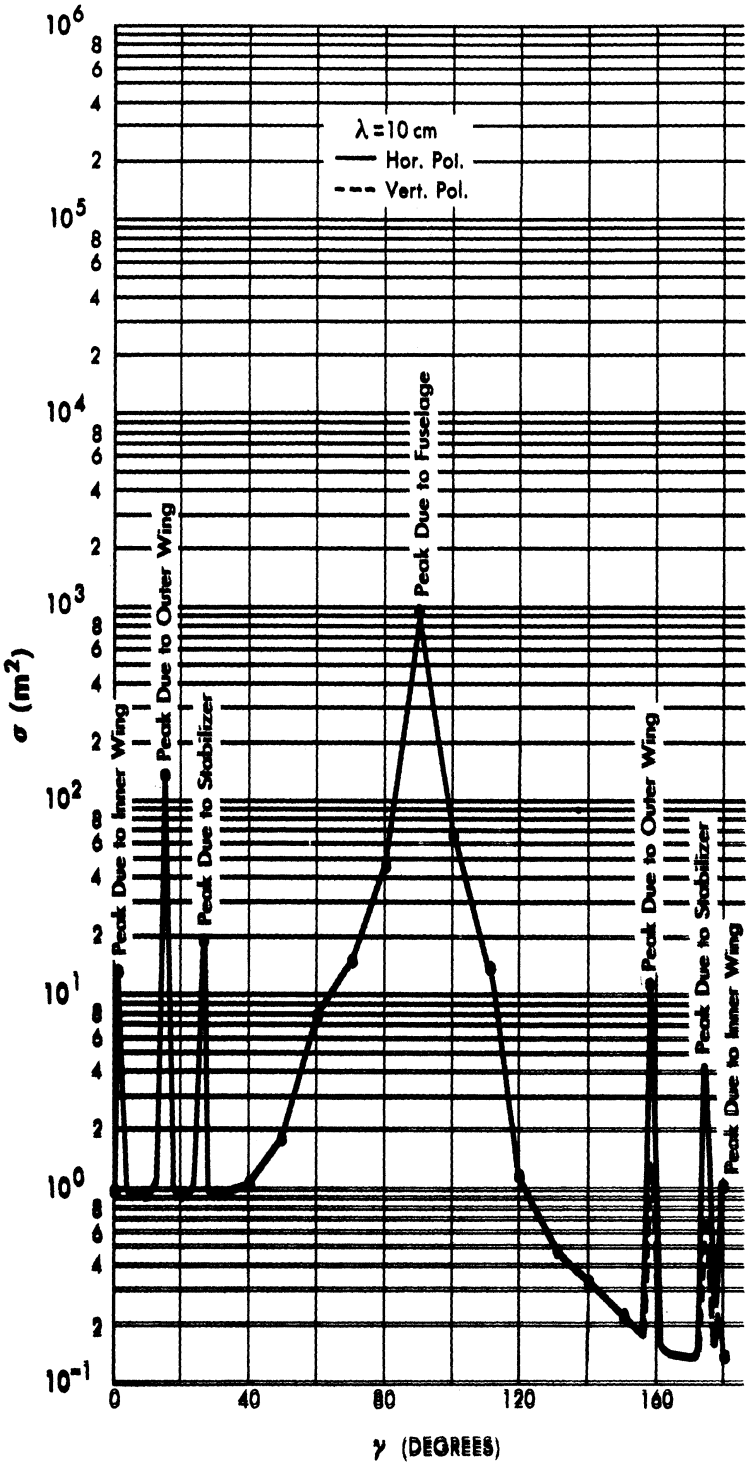

FIG. 2-4 RADAR CROSS-SECTION OF THE B-57 AT S-BAND FOR β=30°

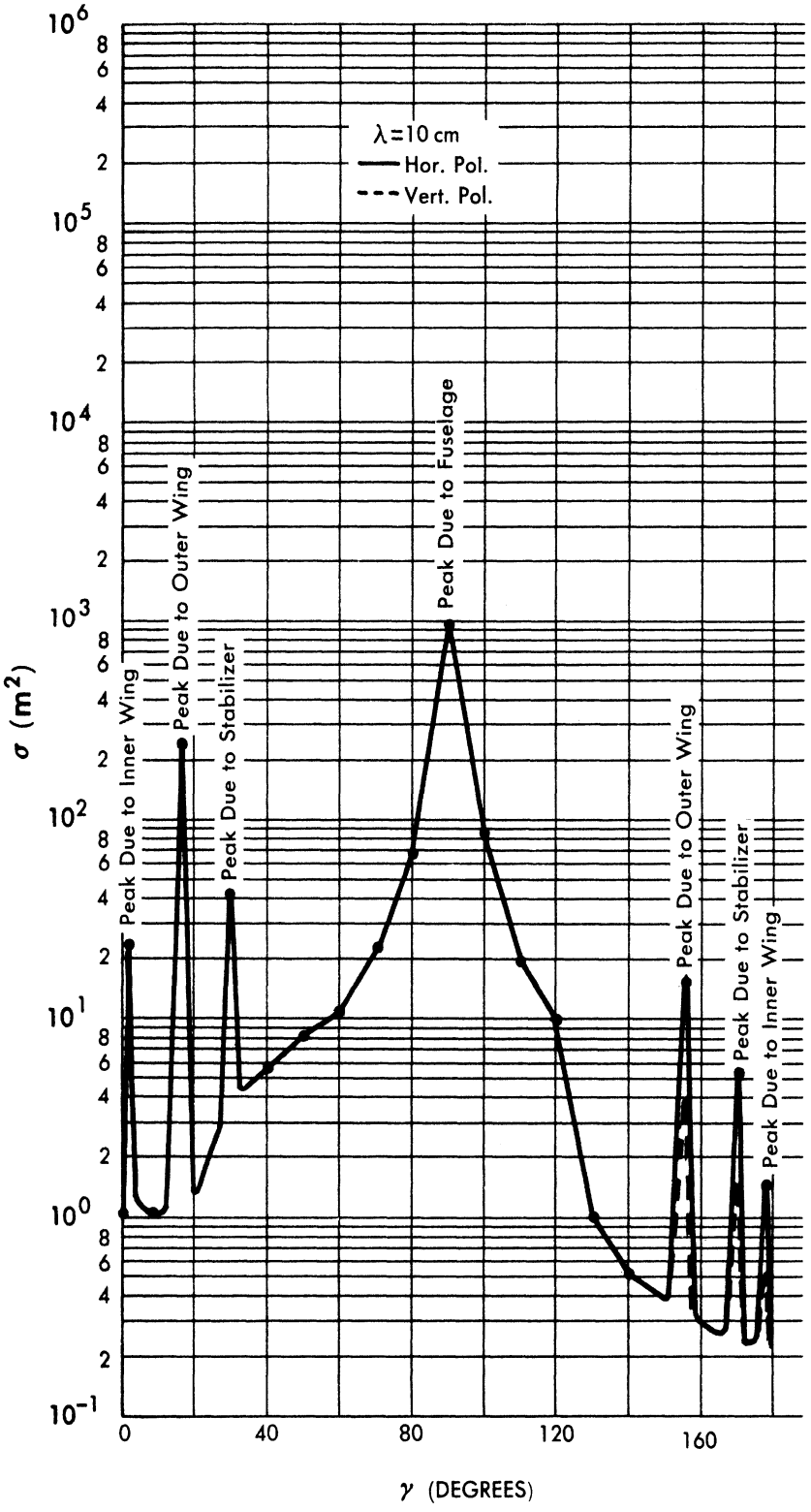

FIG. 2-5 RADAR CROSS-SECTION OF THE B-57 AT S-BAND FOR $\beta = 45°$

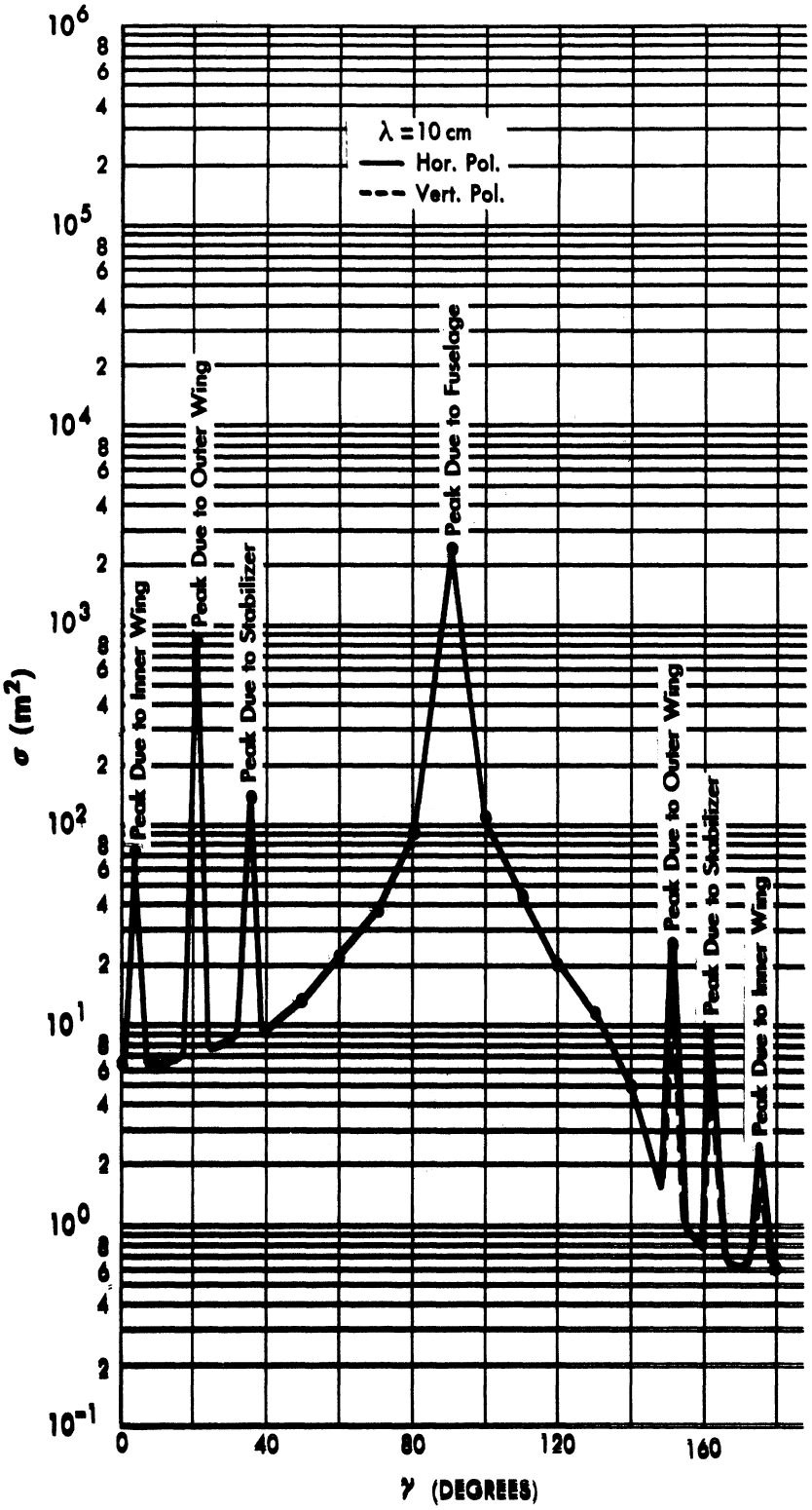

FIG. 2-6 RADAR CROSS-SECTION OF THE B-57 AT S-BAND FOR $\beta = 60°$

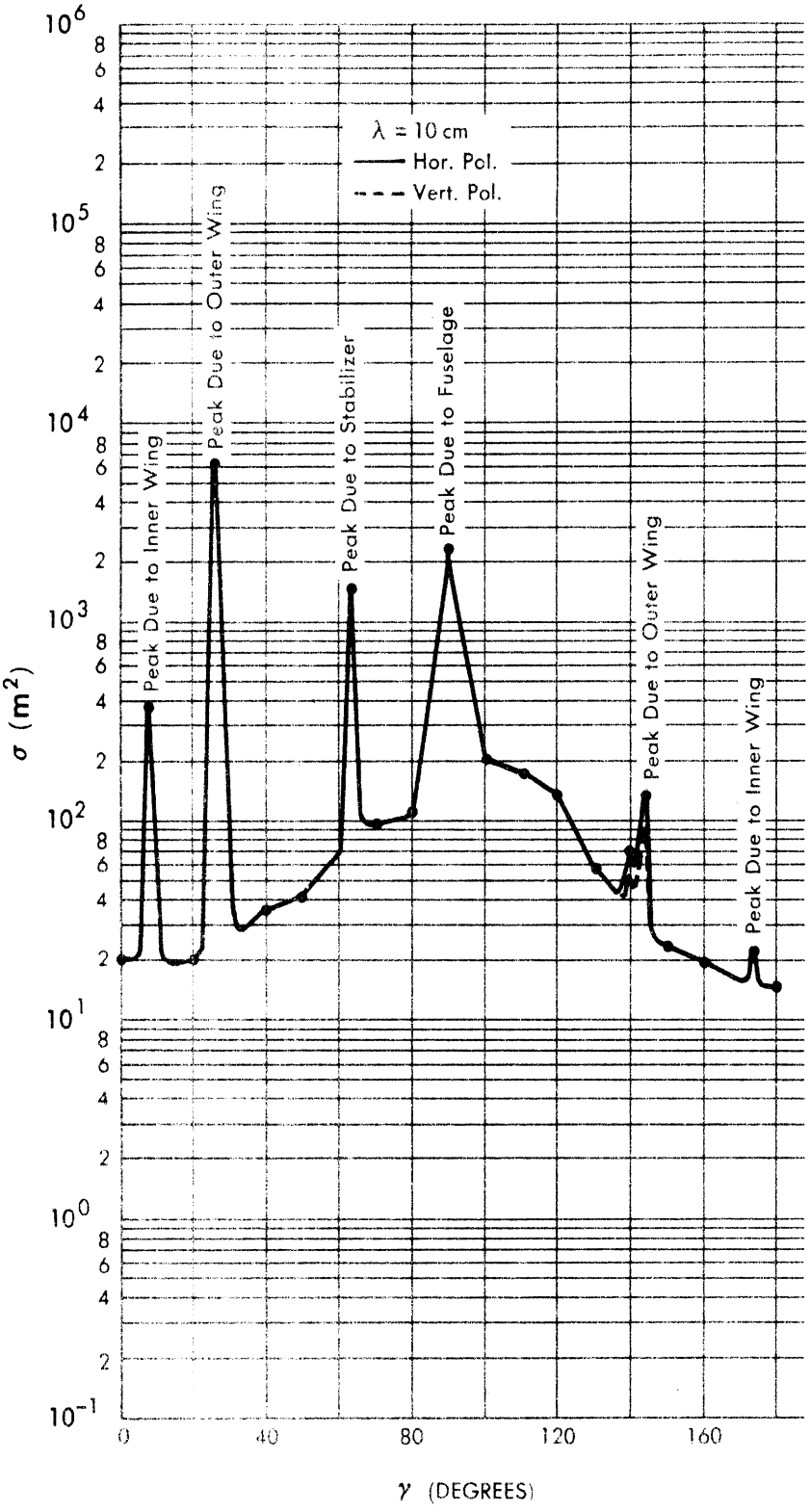

FIG. 2-7 RADAR CROSS-SECTION OF THE B-57 AT S-BAND FOR $\beta = 75°$

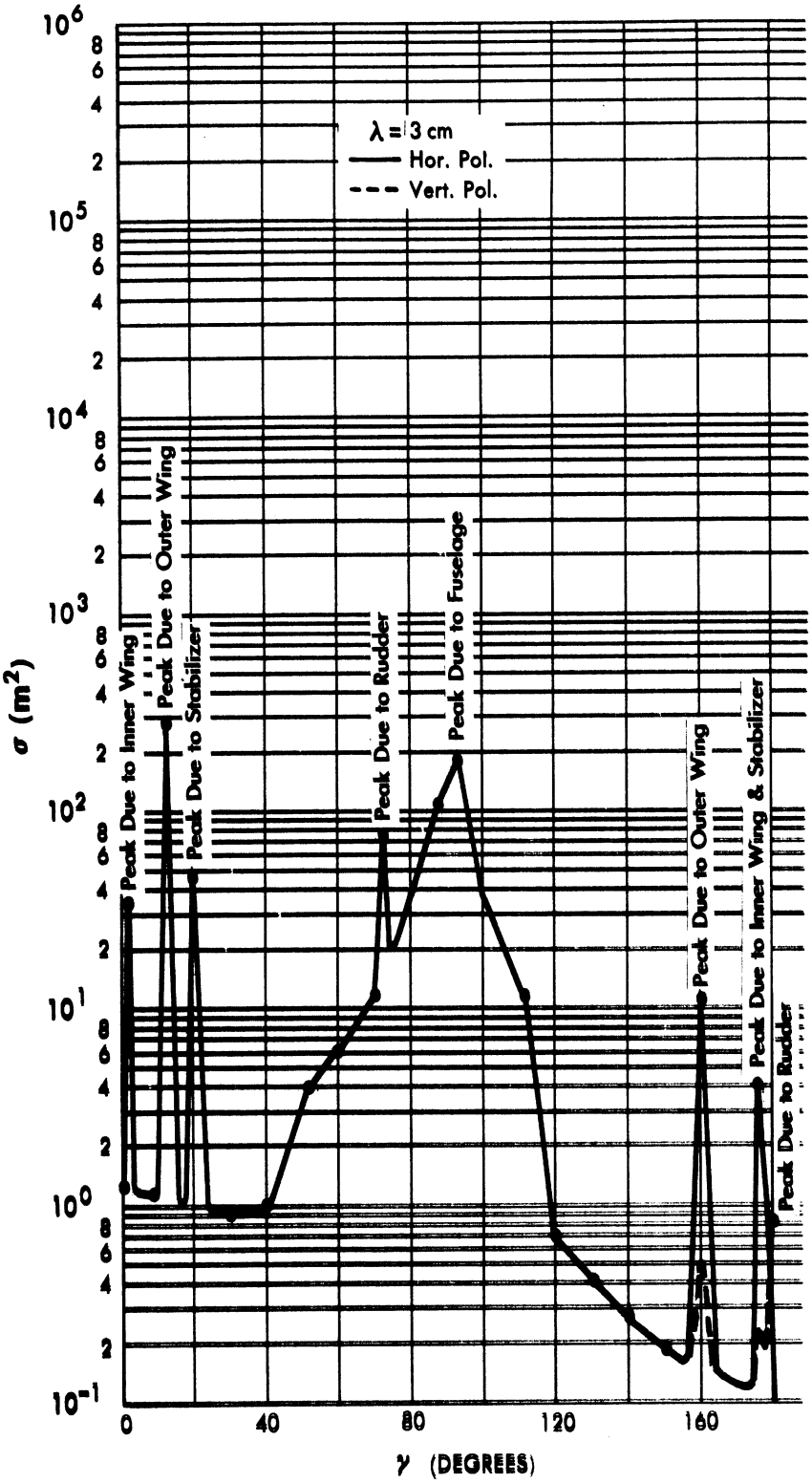

FIG. 2-8 RADAR CROSS-SECTION OF THE B-57 AT X-BAND FOR $\beta = -15°$

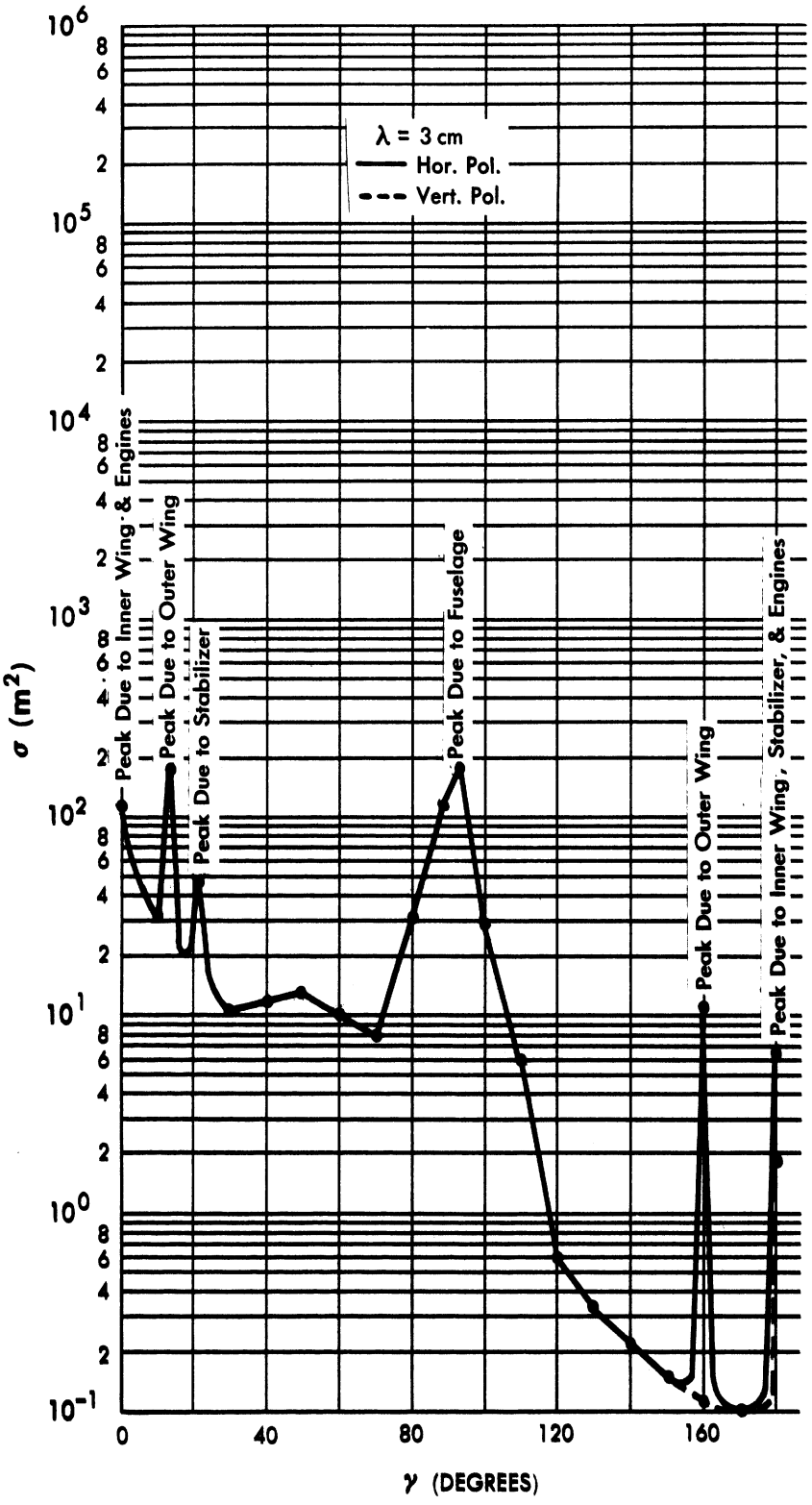

FIG. 2-9 RADAR CROSS-SECTION OF THE B-57 AT X-BAND FOR $\beta = 0°$

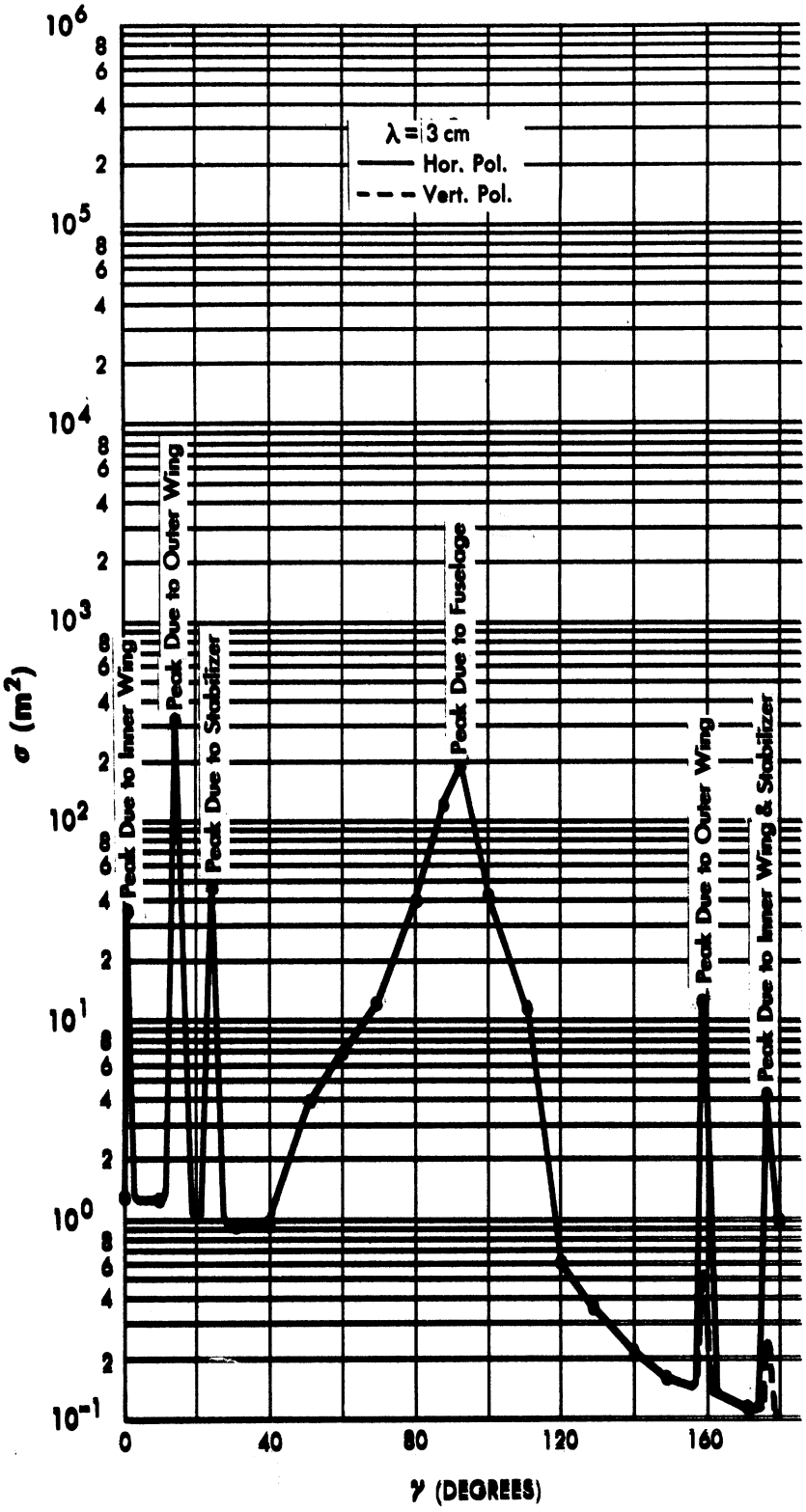

FIG. 2·10 RADAR CROSS-SECTION OF THE B-57 AT X-BAND FOR $\beta = 15°$

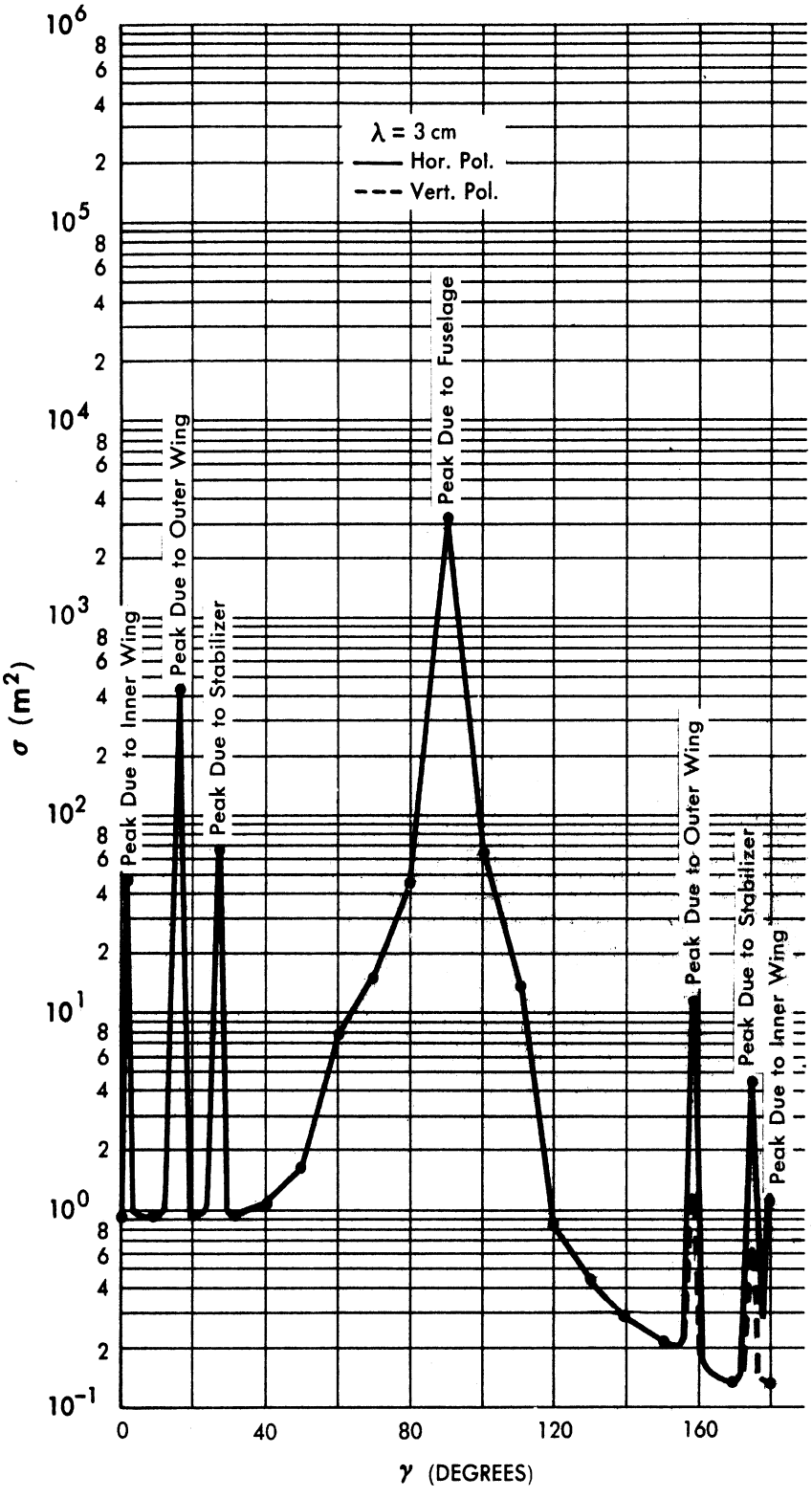

FIG. 2-11 RADAR CROSS-SECTION OF THE B-57 AT X-BAND FOR $\beta = 30°$

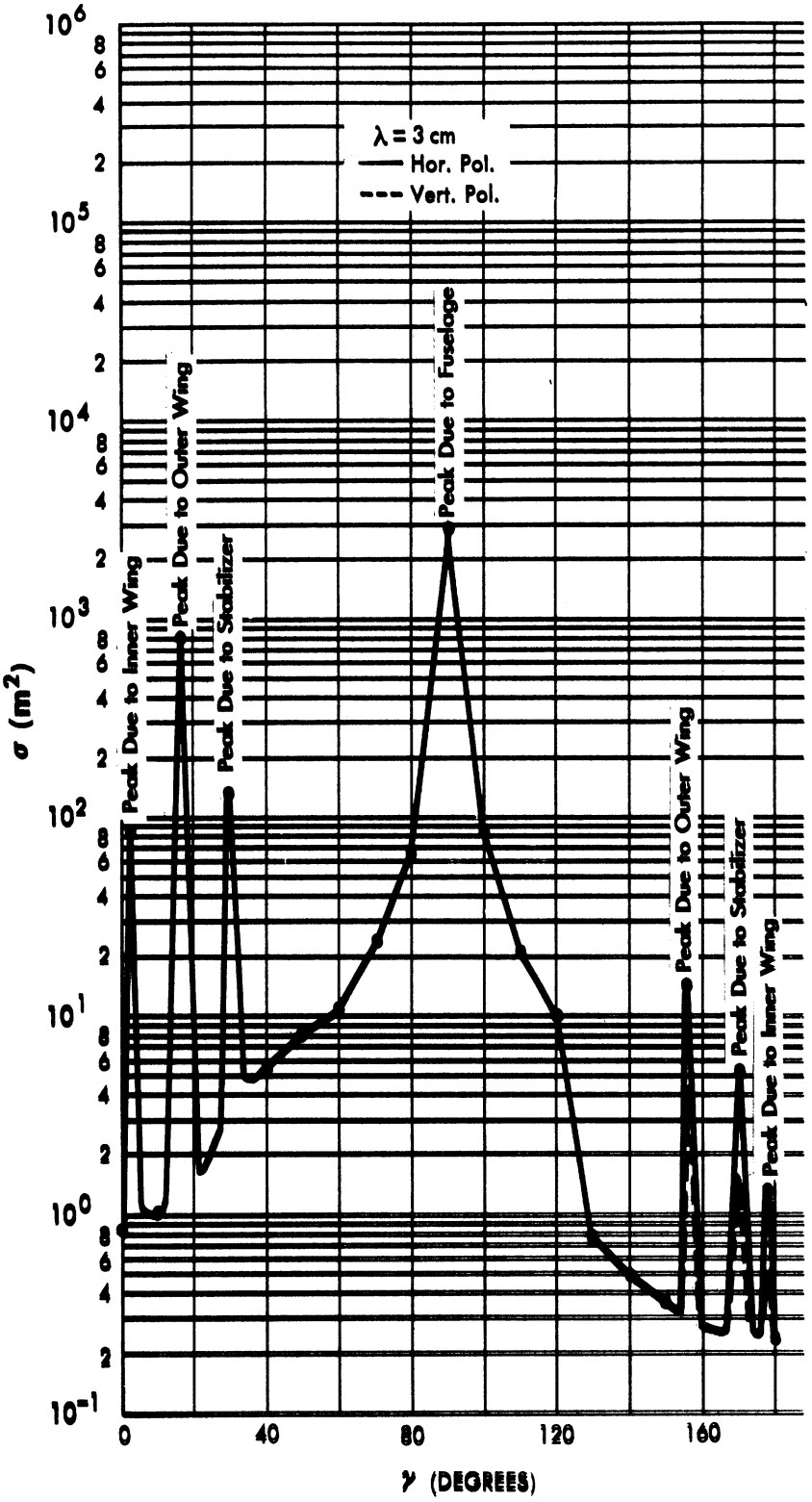

FIG. 2-12 RADAR CROSS-SECTION OF THE B-57 AT X-BAND FOR $\beta = 45°$

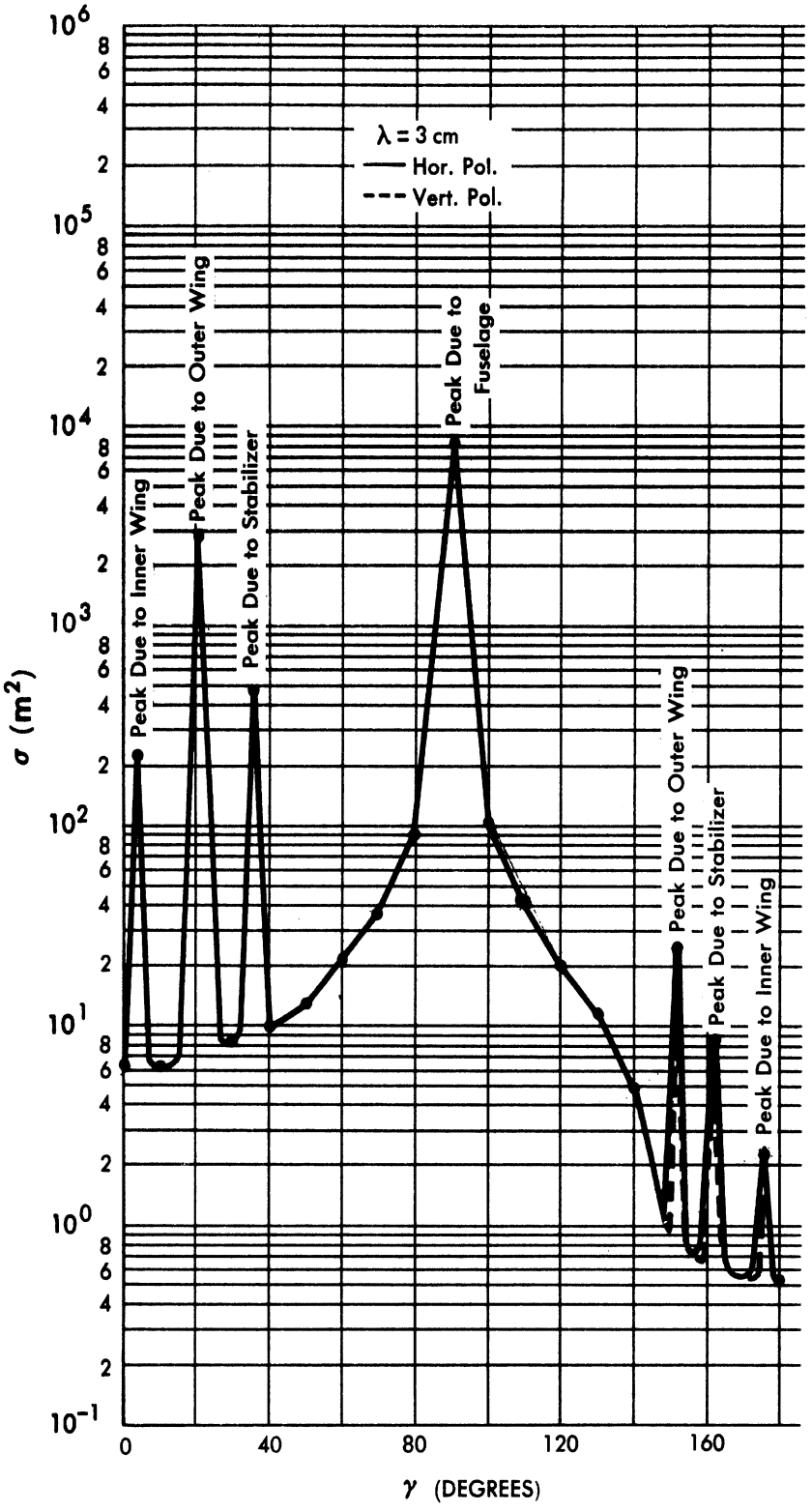

FIG. 2-13 RADAR CROSS-SECTION OF THE B-57 AT X-BAND FOR $\beta = 60°$

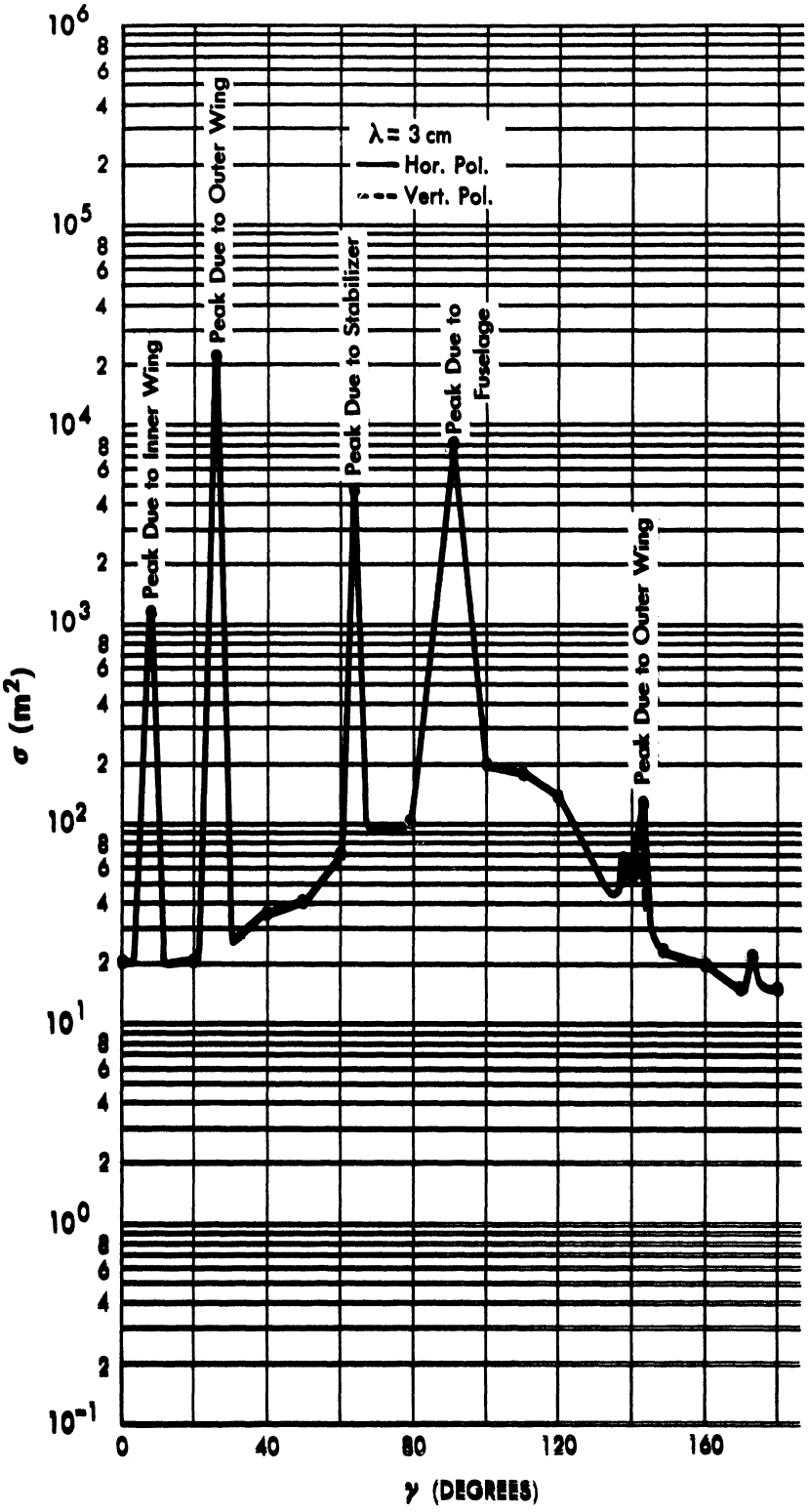

FIG. 2-14 RADAR CROSS-SECTION OF THE B-57 AT X-BAND FOR $\beta = 75°$

Table 2.1

RADAR CROSS-SECTION OF THE B-57 AT X- AND S-BANDS FOR $\beta \approx 90^\circ$

β	cross-section (in m^2)			
	X-band		S-band	
	$\gamma \approx 73^\circ$	$\gamma \approx 79^\circ$	$\gamma \approx 73^\circ$	$\gamma \approx 79^\circ$
79°	8.2×10^3	8.7×10^3	2.5×10^3	2.6×10^3
85°	7.7×10^4	8.2×10^3	2.2×10^4	2.5×10^3
90°	8.2×10^3		2.5×10^3	

III

COMPARISON OF THEORY AND EXPERIMENT

Estimates of the radar cross-section of the B-57 aircraft have been computed as functions of the azimuth and elevation angles for X- and S- bands. It is believed that the values of cross-section given here are for the most part correct to within 6 db. It is to be noted that for some ranges of azimuth angle (notably in the vicinity of sharp peaks) the values of cross-section given here should be considered as allowing a one- or two-degree tolerance in the azimuth angle.

The Telecommunications Research Establishment of England has performed dynamic test measurements of the cross-section of the Canberra B2. The measurements were made at X-band, and the results of the experiment are reported in Reference 3. Their results are for a radar in the plane of level flight ($\beta \approx 0^{\circ}$), and the aspect is given in terms of the bearing of the radar relative to the line of flight of the aircraft (γ). The average values of cross-section reported were derived by weighting each run according to its duration. Their results for the Canberra B2 are shown in Figure 3-1, where these experimental data are compared with the theoretical evaluations reported in Section II.

Examination of Figure 3-1 shows that there is good agreement between theory and experiment at the aspects for which experimental data is available. Apparent discrepancies could easily be due to slight variations in the aspect angles β and γ.

The authors would like to express their thanks to M. L. Barasch and R. E. Kleinman for their assistance in setting up the computations, and to B. Bernstein and A. Nelson for their help during the computational phase of the program.

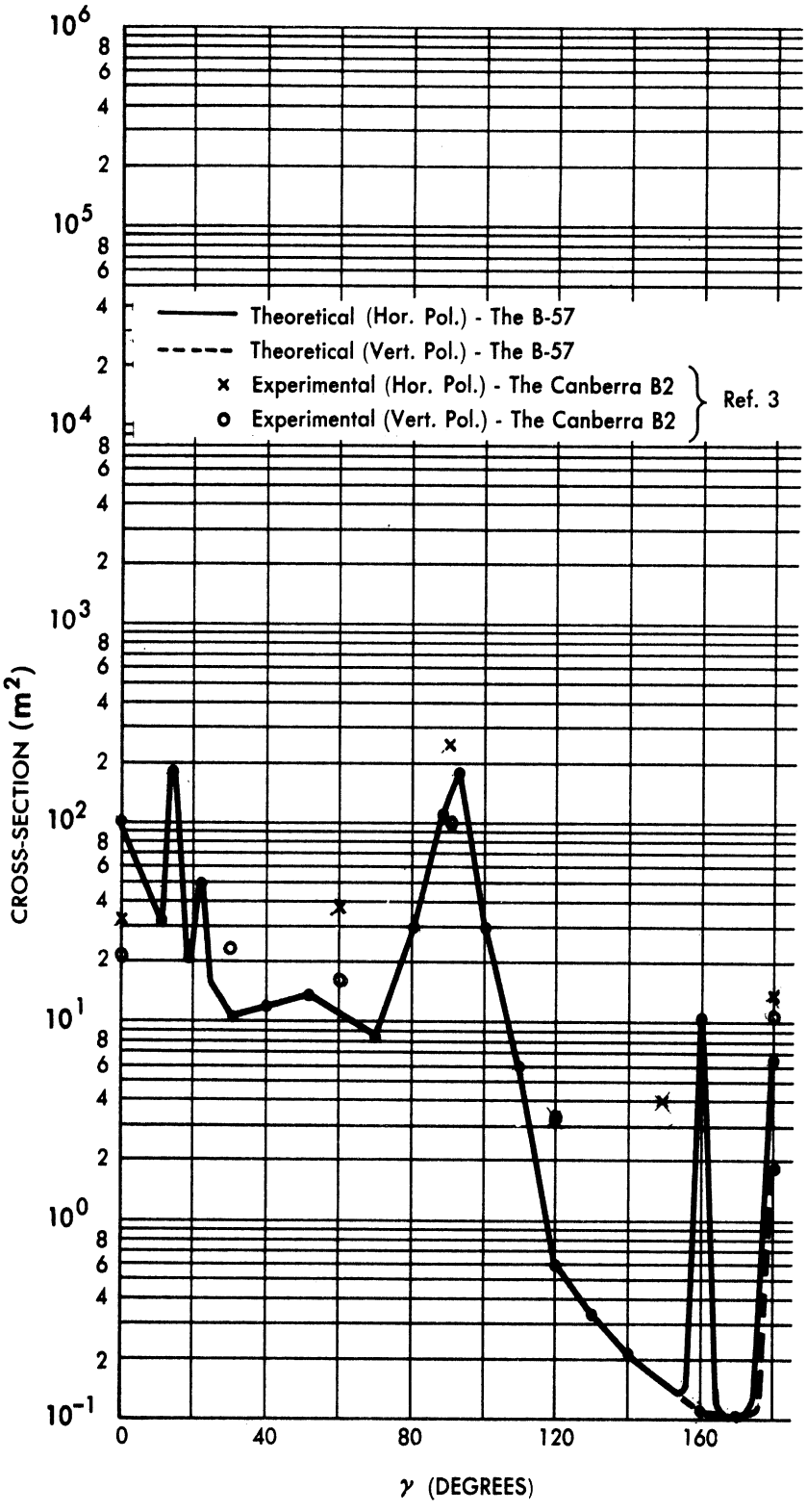

FIG. 3-1 COMPARISON BETWEEN THEORY AND EXPERIMENT AT X-BAND ($\beta = 0°$)

APPENDIX A

GEOMETRICAL BREAKDOWN OF THE AIRCRAFT AND COMPUTATIONAL PROCEDURES

A.1 INTRODUCTION

For the purpose of computing the radar cross-sections of the B-57, the aircraft is broken down into twelve components and each component then replaced by a combination of simple (mathematically speaking) shapes. The components together with the cross-section symbol used to indicate the magnitude of the contribution of each to the cross-section of the aircraft are listed below:

the fuselage (σ_1),

the left wing tank (σ_2),

the left engine (σ_3),

the left inner wing (σ_4),

the left outer wing (σ_5),

the left stabilizer (σ_6),

the rudder (σ_7),

the right wing tank (σ_8),

the right engine (σ_9),

the right inner wing (σ_{10}),

the right outer wing (σ_{11}), and

the right stabilizer (σ_{12}).

Also included is a thirteenth contributor, σ_{13}, representing the contributions of multiple reflections. The remainder of Appendix A is devoted to the further breakdown of each component and to the formulas used in computing the σ_i's. Component coordinate systems are used throughout this appendix, and in each case

the relationship between the component coordinate system and the aircraft coordinate system is given. The aircraft system and a typical component system are shown in Figure A-1.

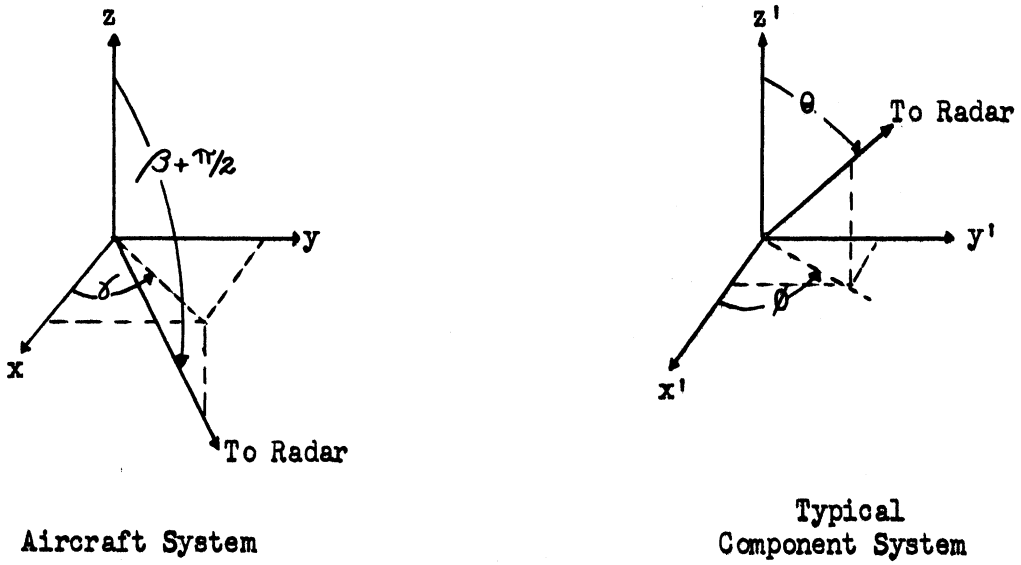

Aircraft System

Typical
Component System

FIG. A-1 COORDINATE SYSTEMS

The cross-section formulas employed are, unless otherwise noted, taken directly from Reference 1. The derivations of these formulas plus a general discussion of the methods of employing them for the determination of the cross-section of an aircraft are given in Appendix A of Reference 1.

The cross-sections were computed at two frequencies (λ= 0.03m and λ= 0.10m) for horizontal and vertical polarizations. A discussion of the shadowing effects and of the combination of the component cross-sections which yield the cross-section of the aircraft itself is presented in Appendix B.

A.2 THE FUSELAGE (σ_1)

The fuselage is considered to consist of five sections: the radome nose, a prolate spheroid, a cylinder, a truncated ogive, and a prolate spheroid (Fig. A-2). Denoting the contribution of the first by $\sigma_{1,1}$, the contribution of the second by $\sigma_{1,2}$, etc., we find that only one of these contributors is of significance at each aspect with which we are concerned.

The radome and front prolate spheroid combined can be approximated by the surface

$$\frac{x'^2 + y'^2}{b^2} + \frac{z'^2}{c^2} = 1 ,$$

with b = 0.99m and c = 6.35m.

The cylinder can be approximated by the surface

$$x'^2 + y'^2 = a^2 ,$$

with a = 0.99m; the length, L, of the cylinder is 3.94m.

The axis of the ogive section is tilted up approximately 4° above the z' axis in the x'z' plane, and the ogive is defined by an arc of a circle of radius 64.8m. The upper portion of the fuselage within the limits of this ogive section could be considered as a truncated cone faired into the ogive; this upper portion will not contribute to the cross-sections computed because the angle of elevation is limited by $\beta \gtrsim -15^\circ$. The radii of the ogive at the truncation planes are 0.99m and 0.34m.

The rear of the fuselage is approximated by a prolate spheroid defined by

$$\frac{x'^2 + y'^2}{b^2} + \frac{z'^2}{c^2} = 1 ,$$

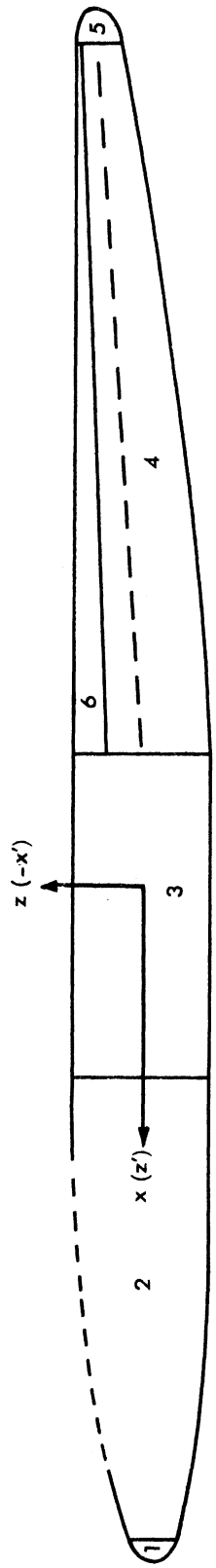

1 - Radome (Prolate Spheroid)
2 - Prolate Spheroid
3 - Cylinder
4 - Ogive
5 - Prolate Spheroid
6 - Truncated Cone (Cross-section Contribution Negligible)

FIG. A-2 BREAKDOWN OF THE FUSELAGE

where b = 0.36m and c = 0.795m. By consideration of the importance of each contributor we see that

$$\begin{aligned}\sigma_1 &= \sigma_{1,1}, \text{ for } 0^\circ \leq \theta < 65^\circ,\\ &= \sigma_{1,2}, \text{ for } 65^\circ < \theta < 90^\circ,\\ &= \sigma_{1,3}, \text{ for } \theta = 90^\circ,\\ &= \sigma_{1,4}, \text{ for } 90^\circ < \theta < 98^\circ, \text{ and}\\ &= \sigma_{1,5}, \text{ for } 98^\circ < \theta \leq 180^\circ,\end{aligned}$$

with $\cos\theta = \cos\beta\cos\gamma$. Formulas for the $\sigma_{1,i}$ are

$$\sigma_{1,2} = \pi b^4 c^2/(c^2\cos^2\theta + b^2\sin^2\theta)^2, \qquad (b = 0.99\text{m and } c = 6.35\text{m})$$

$$\sigma_{1,3} = 2\pi L^2 a/\lambda, \qquad (L = 3.94\text{m and } a = 0.99\text{m})$$

$$\sigma_{1,4} \approx \pi\rho^2\left[1 - \frac{h}{\rho\sin\theta}\right], \qquad (\rho = 64.8\text{m and } h = 63.8\text{m})^*$$

$$\sigma_{1,5} = \pi b^4 c^2/(c^2\cos^2\theta + b^2\sin^2\theta)^2, \qquad (b = 0.36\text{m and } c = 0.795\text{m}).$$

The radome contribution requires a few additional comments. A larger and more detailed drawing of the radome section is shown in Figure A-3.

The surface of the radome is assumed to be completely transparent to the incident energy. Under this assumption the surface irradiated by the incident energy at the join of the radome and fuselage can be approximated by a truncated ogive of half-angle 25° capped by an annulus. The annulus has radii of 0.318m and 0.270m.

*Since the ogive contributes only in the interval $90^\circ < \theta < 98^\circ$, the tilt in the ogive axis is neglected.

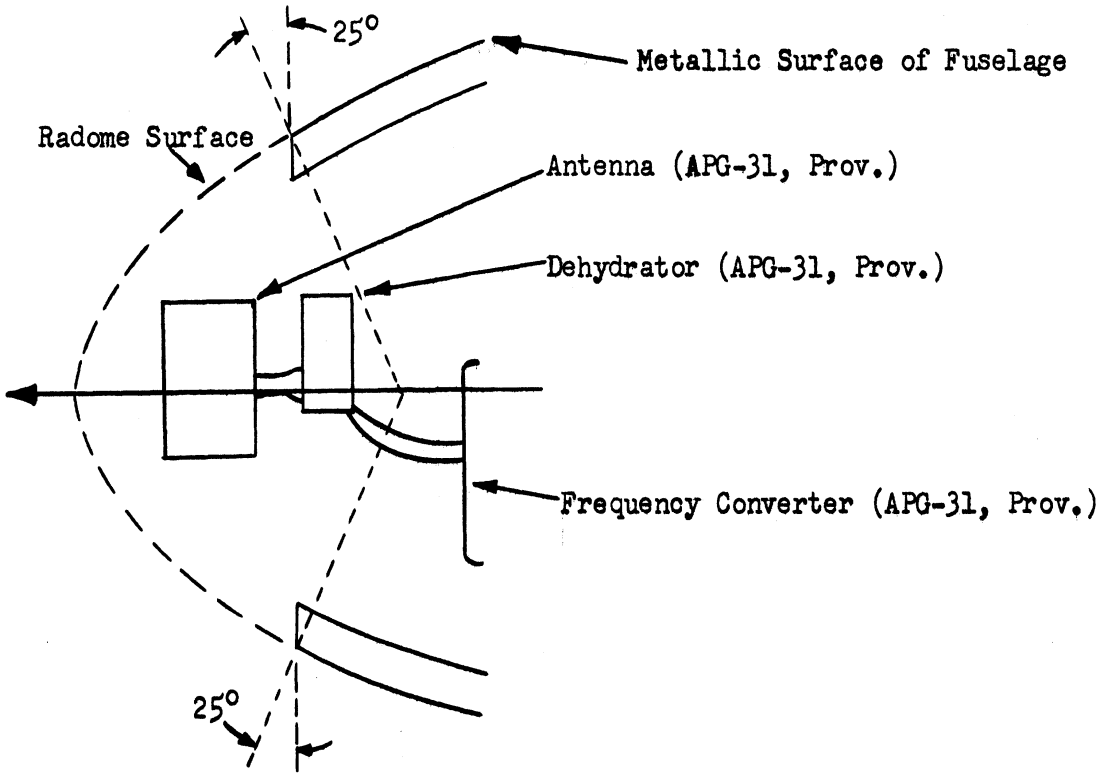

FIG. A-3 BREAKDOWN OF THE RADOME SECTION

The radar equipment covered by the radome and located inside the opening has only been provisionally specified. Thus, because of the uncertainty of the type of the equipment, as well as the size of the equipment, it has been assumed that this equipment and the interior of the opening would scatter in an essentially isotropic fashion. This is approximated by the return from a sphere whose radius is (0.270 cos θ)m. Thus,

$$\sigma_{1,1} = \frac{4\pi \left[\pi(R_1^2 - R_2^2)\right]^2}{\lambda^2} + \frac{\lambda R_1 \left[\tan^2\alpha\right]}{4\pi \sin\theta} + \pi R_2^2, \quad \text{for } \theta = 0^\circ;$$

$$\sigma_{1,1} = \frac{2\left[R_1 + R_2\right]\lambda}{8\pi\sin\theta\tan^2\theta} + \frac{\lambda R_1\left[\tan^2(\theta+\alpha)+\tan^2(\theta-\alpha)\right]}{8\pi\sin\theta} + \pi R_2^{\,2}\cos^2\theta,$$

for $0 < \theta < \alpha$; and

$$\sigma_{1,1} = \frac{2\left[R_1 + R_2\right]\lambda}{8\pi\sin\theta\tan^2\theta} + \frac{\lambda R_1\tan^2(\theta+\alpha)}{8\pi\sin\theta} + \pi R_2^{\,2}\cos^2\theta, \text{ for } \alpha < \theta < 65^\circ;$$

with $\cos\theta = \cos\beta\cos\gamma$. The resulting curve for $\sigma_{1,1}$ is then smoothly faired into the curve for $\sigma_{1,2}$ in the interval $60^\circ < \theta < 70^\circ$.

A.3 THE WING TANKS (σ_2 AND σ_8)

The wing tank is approximated by a prolate spheroid faired into an ogive, as illustrated in Figure A-4.

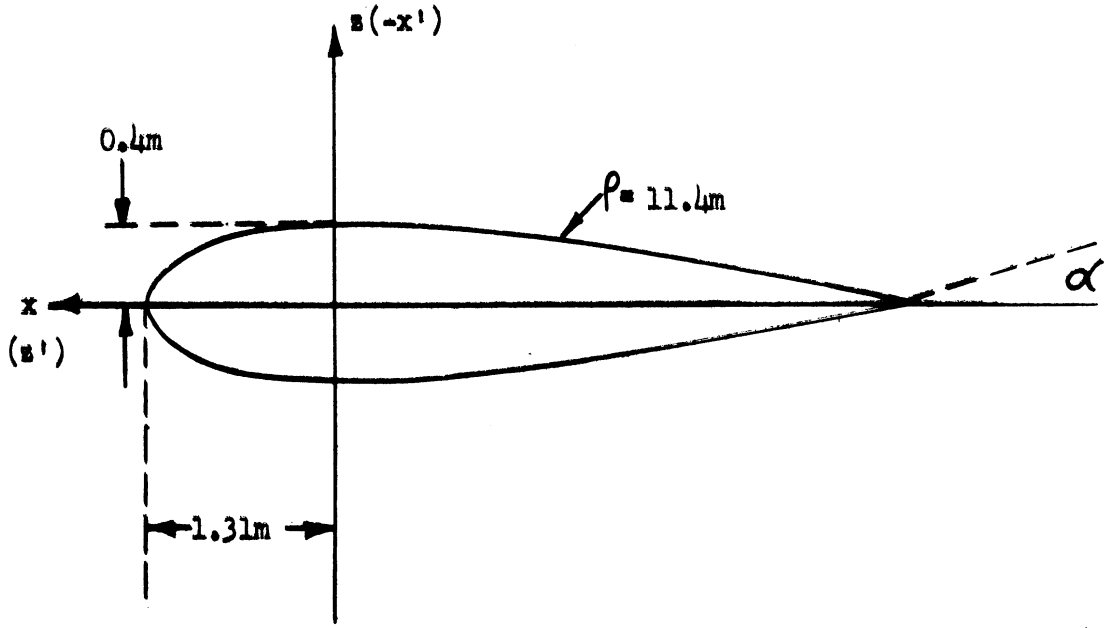

FIG. A-4 BREAKDOWN OF THE WING TANK

The dimensions of these shapes as well as the relationship between the aircraft and the component coordinate systems are shown on the figure.

Since at all aspects (disregarding shadowing for the moment) we have $\sigma_2 = \sigma_8$, it will suffice to define only σ_2. The magnitude of σ_2 as a function of β and γ is given by

$$\sigma_2 = \pi b^4 c^2/(c^2\cos^2\theta + b^2\sin^2\theta)^2, \quad \text{for } 0^\circ \leq \theta < 90^\circ,$$

where b = 0.40m, c = 1.31m, and $\cos\theta = \cos\beta\cos\gamma$; and

$$\sigma_2 = \pi\rho^2\left(1 - \frac{h}{\rho\sin\theta}\right), \quad \text{for } 90^\circ < \theta < 90^\circ + \alpha,$$

$$= \rho^2\sin^2\alpha/4\pi, \quad \text{for } 90^\circ + \alpha = \theta, \text{ and}$$

$$= \frac{\lambda^2\tan^4\alpha}{16\pi\cos^6\theta(1-\tan^2\alpha\tan^2\theta)^3}, \quad \text{for } 90^\circ + \alpha < \theta \leq 180^\circ,$$

where

$\alpha = \cos^{-1}(h/\rho) \approx 15^\circ$,

$\rho = 11.4$m,

h = 11.0m, and

$\cos\theta = \cos\beta\cos\gamma$.

A.4 THE ENGINES (σ_3 AND σ_9)

From the front the engine is considered to consist of a torus surface with a small prolate spheroid located in the center. The outer radius of the torus is 0.39m and the inner radius is 0.29m. The prolate spheroid has a semi-major axis of 0.25m and a semi-minor axis of 0.20m (only half of the semi-major axis is visible when viewed from the side of the aircraft). Viewed from the side, the engine is considered to consist of a truncated ogive, a cylinder, and a second truncated ogive. (The top of the engine is not cylindrical; however, for

those aspects for which the top of the engine would be considered, the stationary phase point on the surface of the engine would be inside the wing and thus would not contribute to the cross-section.)

The front ogive has radii of 0.60m and 0.39m at the truncation planes, and the truncation planes are 0.82m apart. The cylinder has a radius of 0.60m and a length of 4.48m. The rear ogive has radii of 0.60m and 0.29m at the truncation planes.

Viewed from the rear, the engine is considered to consist of three sharp edges (modeled as wire loops) of radii 0.29m, 0.28m, and 0.21m. The structure back in the interior of the "hole" (in the case of the F-94C this is about 6 feet inside the hole) is approximated by three wire loops of radii ranging from 0.14m to 0.15m.

This breakdown is illustrated in Figure A-5.

Neglecting shadowing effects for the moment, it is seen from the aircraft drawings that $\sigma_3 \equiv \sigma_9$. Thus, it will suffice to restrict our attention to σ_3.

With the z' axis coincident with the x axis and the y' axis coincident with the y axis, the breakdown of the engine described above and illustrated in Figure A-5 leads to the following expressions for σ_3:

$0^\circ < \theta < 53^\circ$

$$\sigma_3 \equiv A + \left[\pi (b')^4 (a')^2\right] \Big/ \left[(a')^2 \cos^2\theta + (b')^2 \sin^2\theta\right]^2,$$

where $A \equiv 8\pi ab^2/\lambda$, for $\theta \equiv 0^\circ$,

$\equiv 2\pi ab/\sin\theta$, for $0^\circ < \theta < 53^\circ$,

and $a = 0.05m$, $b' = 0.20m$,

$b = 0.34m$, $a' = 0.25m$, and $\cos\theta = \cos\beta \cos\gamma$.

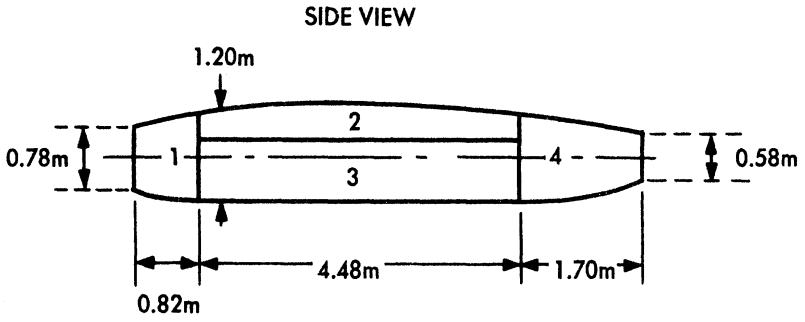

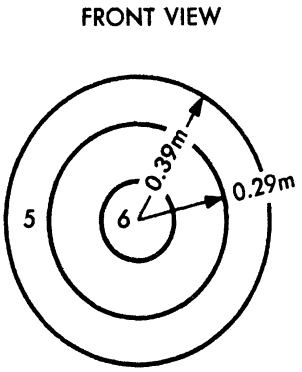

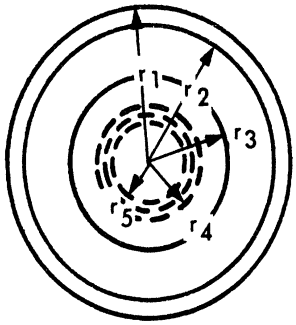

(All wire loops)

$r_1 = 0.29m$

$r_2 = 0.28m$

$r_3 = 0.21m$

$r_4 = 0.15m$

$r_5 = 0.14m$

1 - A Truncated Ogive
2 - An Ogive Faired into the Cylinder (Contribution Negligible)
3 - A Cylinder
4 - An Ogive
5 - A Torus
6 - A Prolate Spheroid

FIG. A-5 BREAKDOWN OF THE ENGINE

$53^\circ < \theta < 90^\circ$

$$\sigma_3 = \pi\rho^2\left[1 - \frac{h}{\rho\sin\theta}\right] ,$$

where $\rho = 1.71m$,

$h = 1.11m$, and $\cos\theta = \cos\beta\cos\gamma$.

$\theta = 90^\circ$

$$\sigma_3 = 2\pi L^2 a/\lambda ,$$

where $L = 4.48m$, and $a = 0.60m$.

$90^\circ < \theta < 112^\circ$

$$\sigma_3 = \pi\rho^2\left[1 - \frac{h}{\rho\sin\theta}\right] ,$$

where $\rho = 4.82m$,

$h = 4.22m$, and

$\cos\theta = \cos\beta\cos\gamma$.

$112^\circ < \theta < 158^\circ$

$$\sigma_3 = \frac{\lambda a}{8\pi\sin\theta}\left[\tan^2(\theta - 22^\circ)\right] ,$$

where $a = 0.29m$, and $\cos\theta = \cos\beta\cos\gamma$.

$158^\circ < \theta < 180^\circ$

$$\sigma_3 = \frac{\lambda a}{8\pi\sin\theta}\left[\tan^2(\theta + 22^\circ) + \tan^2(\theta - 22^\circ)\right] ,$$

where $a = 0.29m$, and $\cos\theta = \cos\beta\cos\gamma$.

$\theta = 180^\circ$

$$\sigma_3 = \pi a^2\tan^2(22^\circ) + \pi\sum_{i=1}^{6}(r_i)^2 ,$$

where $a = r_1 = 0.29m$,

$r_2 = 0.28m$,

$r_3 = 0.21m$,

$r_4 = 0.15m$,

$r_5 = 0.145m$, and

$r_6 = 0.14m$.

A.5 WING, STABILIZER, AND RUDDER SURFACES

Each inner wing (σ_4 and σ_{10}) is considered to be composed of an elliptic cylinder faired into a tapered wedge. The outer wing (σ_5 and σ_{11}), stabilizer (σ_6 and σ_{12}), and rudder (σ_7) surfaces are each considered to consist of a truncated elliptic cone faired into a tapered wedge with the "wing-tip" approximated by an ellipsoid.

In terms of their coordinate systems the elliptic cylinder contribution is given by

$$\sigma_a = \frac{2\pi L^2 a^2 b^2}{\lambda(a^2\cos^2\phi + b^2\sin^2\phi)^{3/2}}, \quad \text{for } \theta = 90^\circ;$$

for $\theta \neq 90^\circ$ the contribution is negligible. The coordinate system and the meaning of the parameters is shown in Figure A-6.

The contribution from the truncated elliptic cone is negligible except at the aspects defined by

$$\tan\theta = \frac{-\eta}{\tan\alpha\sqrt{\sin^2\phi + \eta^2\cos^2\phi}}.$$

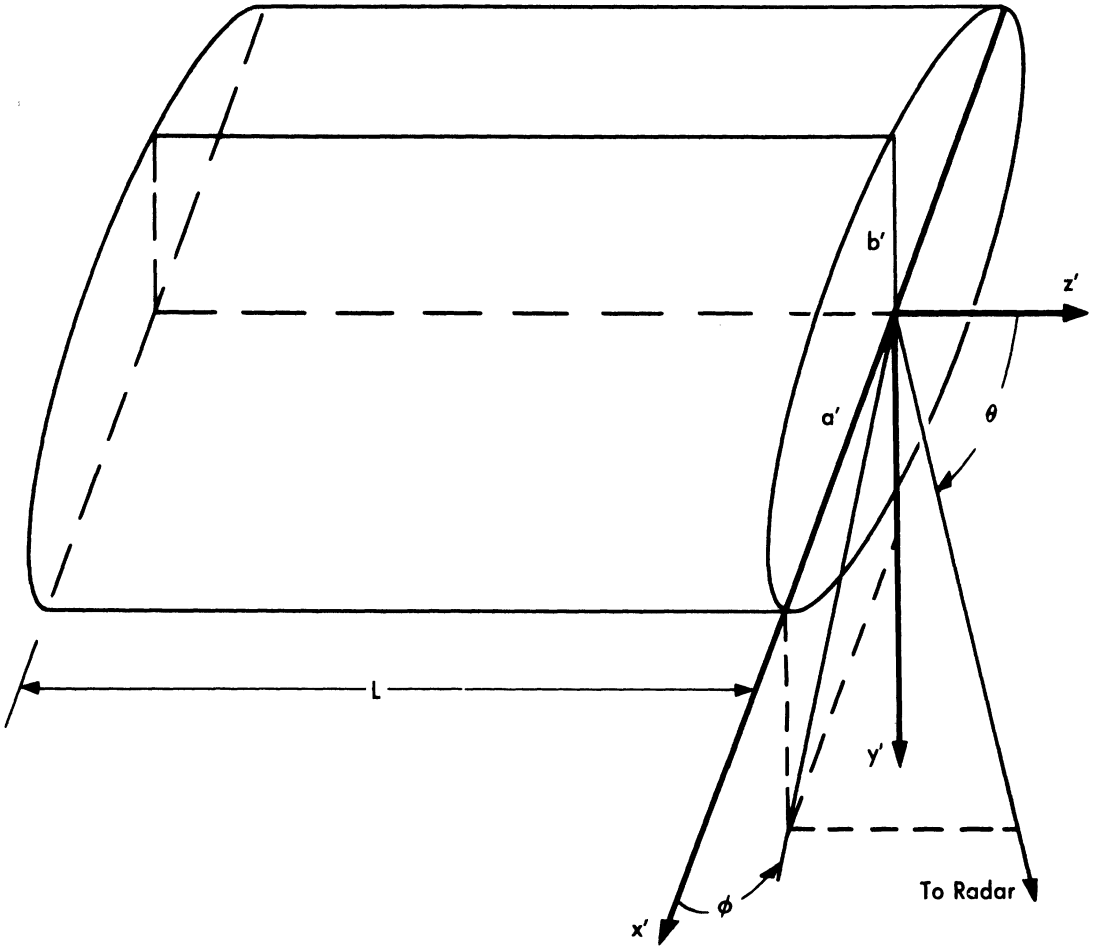

FIG. A-6 THE ELLIPTIC CYLINDER

At these aspects the cross-section contribution is given by

$$\sigma_b = \frac{8\pi\left[(L_2)^{3/2}-(L_1)^{3/2}\right]^2 \tan^4\alpha}{9\lambda\eta^2\left|\cos^3\theta\right|} .$$

The coordinate system and the meaning of these parameters is shown in Figure A-7.

The spheroid cap contribution is given by

$$\sigma_c = \frac{\pi(a'b'c')^2}{\left[(a')^2\sin^2\theta\cos^2\phi+(b')^2\sin^2\theta\sin^2\phi+(c')^2\cos^2\theta\right]^2} ,$$

with the coordinate system and parameters as shown in Figure A-8.

The tapered wedge contribution is given by

$$\sigma_d = \frac{\pi L^2\cos^4\psi}{(\pi-\alpha)^2} + A ,$$

where

$$A = \frac{L^2\tan^2(\alpha+\theta)}{4\pi}, \text{ for } \alpha<\theta<\frac{\pi}{2}-\alpha ,$$

$$= \frac{L^2\sin^2(2\alpha)}{4\pi\cos^2(\alpha-\theta)\cos^2(\alpha+\theta)}, \text{ for } 0^\circ\leq\theta<\alpha , \text{ and}$$

ψ = the angle between the polarization vector and the plane formed by the direction of incidence and the edge of the wedge;

the remaining parameters and the coordinate system are shown in Figure A-9.

Since the contributions from the right wing surfaces can be obtained by symmetry from the contributions from the left surfaces, it will suffice here to restrict our attention to σ_4, σ_5, σ_6, and σ_7.

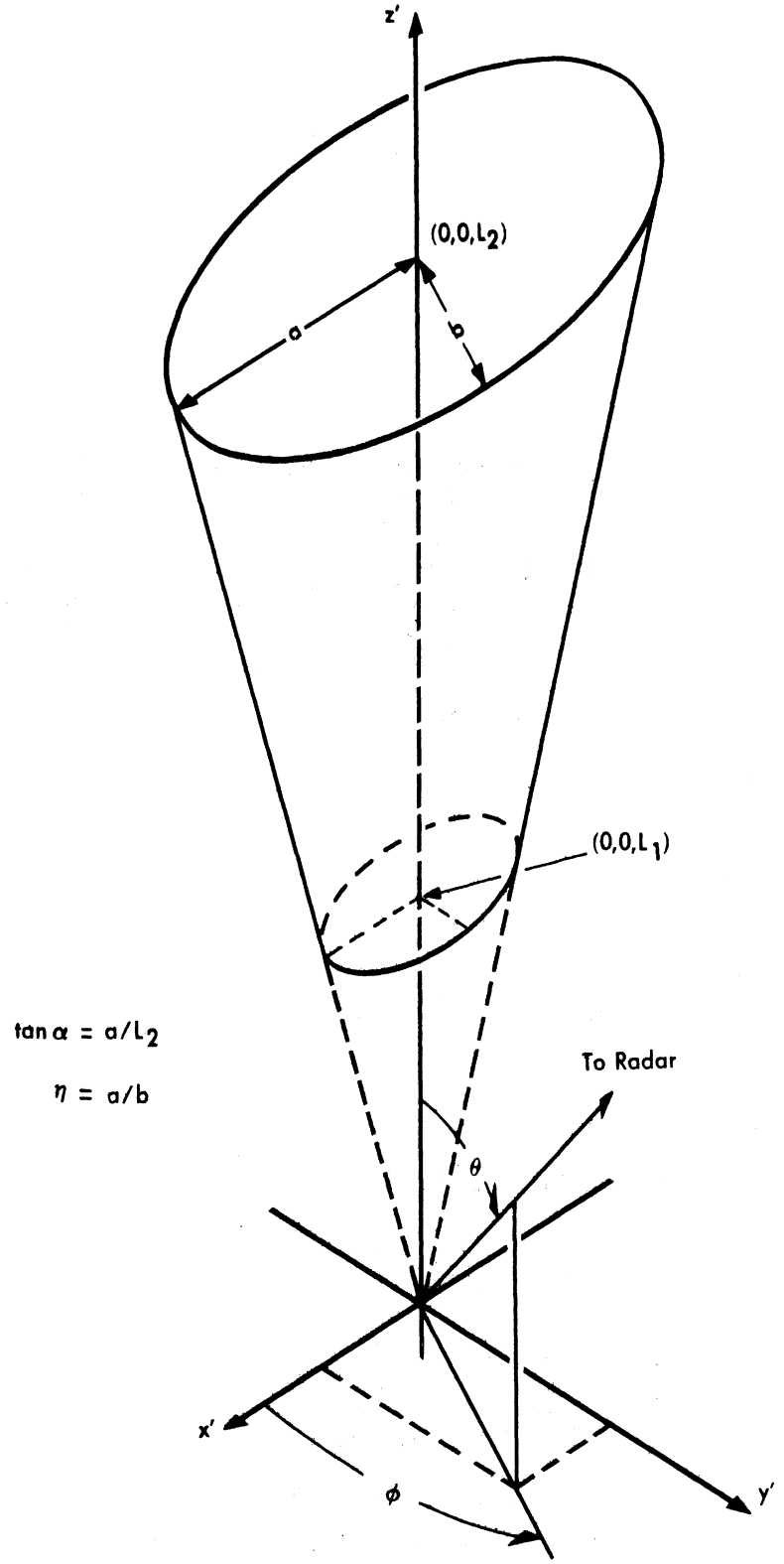

FIG. A-7 THE TRUNCATED ELLIPTIC CONE

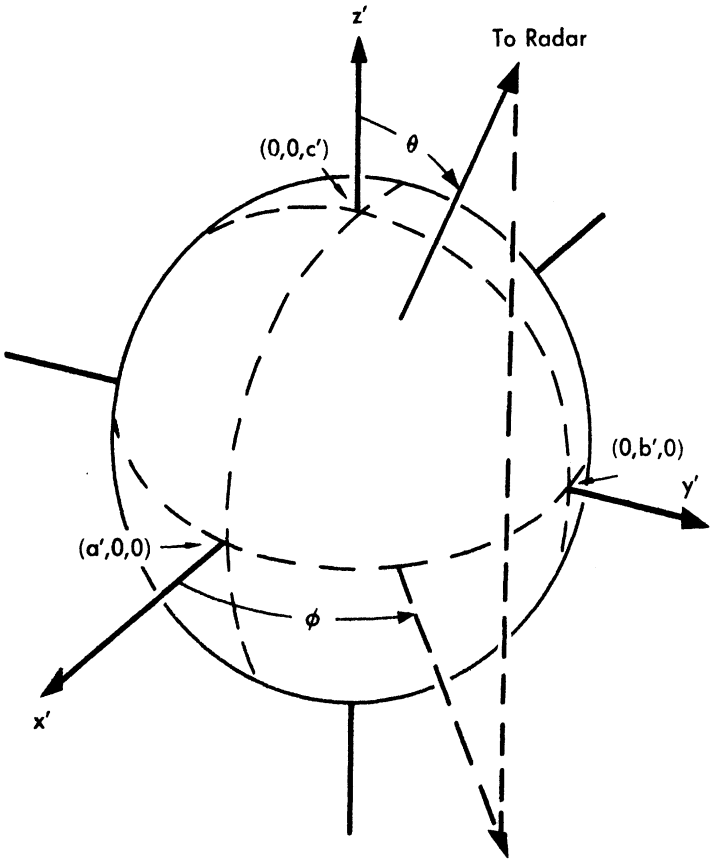

FIG. A-8 THE ELLIPSOID

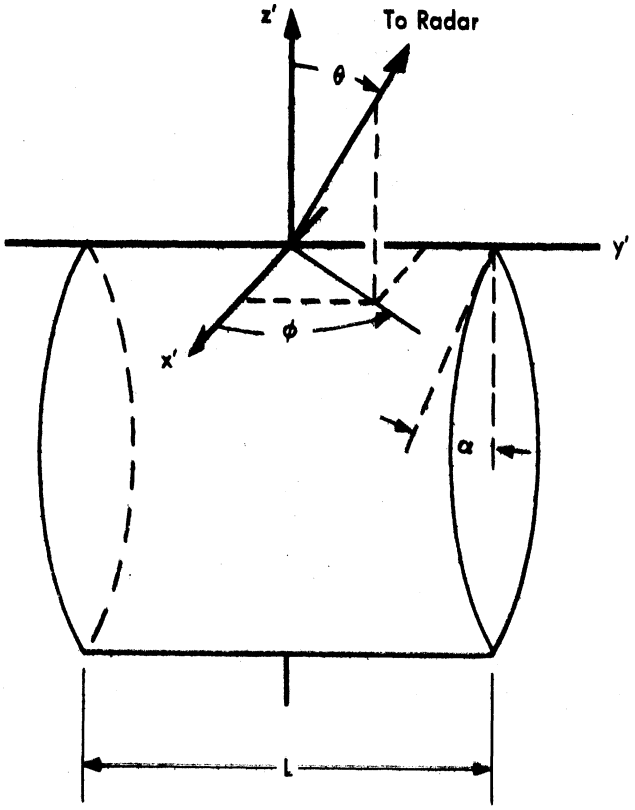

FIG. A-9 THE TAPERED WEDGE

The left inner wing

The elliptic cylinder of length, L, located in the front is defined by

$$(x'/a')^2 + (y'/b')^2 = 1,$$

where a' = 2.31m, b' = 0.348m, and L = 1.69m.

The tapered wedge has a length, L, of 1.69m, and a half-angle, α, of 5°.

The relationship between the cylinder coordinate system and the aircraft coordinate system is given by

$$\sin\beta \simeq \cos(2^\circ)\sin\phi,$$

$$\tan\gamma \simeq \sin(2^\circ)\tan\phi.$$

With regard to the edge of the wedge, the direction of incidence is normal to the edge if

$$\sin\gamma \simeq \tan(2^\circ)\tan\beta,$$

and thus the relationship $\beta \simeq \theta$ is used in relating the component coordinate system to the aircraft system in this normal plane.

The left outer wing

The truncated elliptic cone is defined by

$$a = 2.31m, \quad L_1 = 3.89m, \quad \alpha = 13.5^\circ;$$

$$b = 0.348m, \quad L_2 = 9.56m, \quad \eta = 6.66.$$

The tapered wedge has a length of 6.04m, and a half angle of 5°.

The ellipsoid cap is defined by

$$(x'/a')^2 + (y'/b')^2 + (z'/c')^2 = 1,$$

where a' = 1.17m, b' = 0.142m, and c' = 0.567m.

For the ellipsoid and the cone the relation between the component coordinate system and the aircraft system is given by

$$\sin\beta = -\sin(2^\circ)\cos(4^\circ 21')\sin\theta\cos\phi - \cos(2^\circ)\cos(4^\circ 21')\sin\theta\sin\phi + \sin(4^\circ 21')\cos\theta;$$

$$\cos\beta\cos\gamma = \cos(2^\circ)\sin\theta\cos\phi - \sin(2^\circ)\sin\theta\sin\phi;$$

$$\cos\beta\sin\gamma = -\sin(2^\circ)\sin(4^\circ 21')\sin\theta\cos\phi - \cos(2^\circ)\sin(4^\circ 21')\sin\theta\sin\phi - \cos(4^\circ 21')\cos\theta.$$

For the tapered wedge the direction of normal incidence to the edge is given by

$$\cos(\gamma - 70^\circ) \approx \tan(4^\circ 21')\tan\beta,$$

and the relation $\beta = \theta$ in this plane is used to relate the component system to the aircraft system.

The left stabilizer

The truncated elliptic cone is given by

$$a = 1.40\text{m}, \quad L_1 = 3.00\text{m}, \quad \alpha = 12^\circ;$$

$$b = 0.168\text{m}, \quad L_2 = 6.58\text{m}, \quad \eta = 8.35.$$

The tapered wedge has a length of 3.58m and a half-angle of 5°.

The ellipsoid cap is given by

$$(x'/a')^2 + (y'/b')^2 + (z'/c')^2 = 1,$$

where $a' = 0.635\text{m}$, $b' = 0.076\text{m}$, and $c' = 0.380\text{m}$.

For the ellipsoid and the cone the relation between the component coordinate system and the aircraft system is given by

$$\sin\beta = -\cos(9^\circ 45')\sin\theta\sin\phi + \sin(9^\circ 45')\cos\theta;$$

$$\tan\gamma = \frac{A\sin(12^\circ) - B\sin(9^\circ 45')\cos(12^\circ) - C\cos(9^\circ 45')\cos(12^\circ)}{A\cos(12^\circ) - B\sin(9^\circ 45')\sin(12^\circ) - C\cos(9^\circ 45')\sin(12^\circ)},$$

where $A = \sin\theta\cos\phi$, $B = \sin\theta\sin\phi$, $C = \cos\theta$.

The direction of normal incidence to the edge of the wedge is given by

$$\sin\gamma \approx \tan(10^\circ)\tan\beta,$$

and the relation $\beta = \theta$ is used to relate the two coordinate systems in this plane.

The rudder

The elliptic cone is given by

$$a = 1.69\text{m}, \quad L_1 = 1.65\text{m}, \quad \alpha = 27.5^\circ;$$

$$b = 0.147\text{m}, \quad L_2 = 3.06\text{m}, \quad \eta = 11.4.$$

The tapered wedge has a length of 1.59m and a half-angle of 5°.

The ellipsoid cap is given by $a' = c' = 0.079\text{m}$, and $b' = 0.91\text{m}$.

For the cone and the ellipsoid the relationship between the two coordinate systems is given by

$$\sin\beta = \cos(77.5^\circ)\sin\theta\cos\phi + \cos(12.5^\circ)\cos\theta;$$

$$\cos\beta\cos\gamma = -\cos(12.5^\circ)\sin\theta\cos\phi + \cos(77.5^\circ)\cos\theta;$$

$$\cos\beta\sin\gamma = \sin\theta\sin\phi.$$

For the wedge normal incidence is given by

$$\cos\gamma = \cot(15^\circ)\tan\beta,$$

and the relation $\beta = \theta$ is used to relate the wedge coordinate system to the aircraft coordinate system.

A.6 MULTIPLE REFLECTIONS (σ_{13})

Only double reflections are considered in this examination of the effect of multiple scattering on the cross-section of the B-57 aircraft. This restriction is not a serious one since an examination of the aircraft drawings displays a definite absence of "corner reflectors".

The methods of geometric optics are applied in this analysis. Extensive use is also made of the material of Reference 2, wherein multiple scattering by N bodies is discussed. Taking N = 2 and approximating each pair of B-57 components in the vicinity of the reflecting points by the surfaces

$$\frac{x_i^2}{2\rho_{i1}} + \frac{y_i^2}{2\rho_{i2}} = -z_i, \quad (i = 1,2),$$

where the z_i axes are oriented in the direction of the normals to the surfaces (thus $\hat{i}_{z_1} \cdot \hat{i}_{z_2} = 0$*) and

$$\hat{i}_{x_1} \cdot \hat{i}_{x_2} = 1; \; \hat{i}_{x_1} \cdot \hat{i}_{y_1} = \hat{i}_{y_1} \cdot \hat{i}_{x_2} = \hat{i}_{y_1} \cdot \hat{i}_{y_2} = 0,$$

the material of Reference 2 indicates that the double-reflection contribution to the cross-section, σ_d, is given by

$$\sigma_d = \frac{\pi \rho_{11} \rho_{12} \rho_{21} \rho_{22}}{R^2 \sin(2\xi)\left[\sin(2\xi) + \frac{\rho_{21}}{R}\cos\xi + \frac{\rho_{11}}{R}\sin\xi\right]\left[2 + \frac{\rho_{12}}{R}\cos\xi + \frac{\rho_{22}}{R}\sin\xi\right]} \quad \text{(A.6-1)}$$

---

* In order for the reflected ray to return in the direction from which it came it is necessary that the normals to the two surfaces at the reflecting points be perpendicular.

The geometry of the situation as well as graphical definitions of the parameters ξ and R are given in Figure A-10.

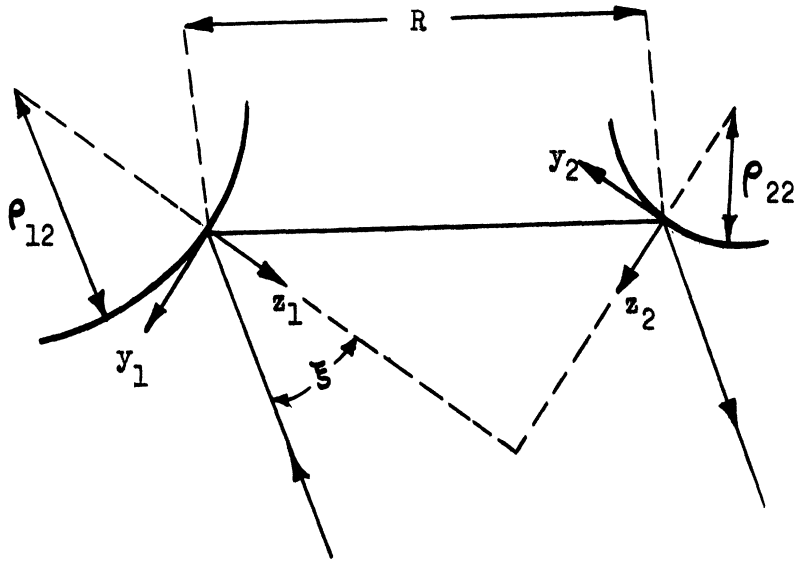

FIG. A-10 DOUBLE REFLECTIONS (showing one of the two rays; the other ray follows the reverse path)

In the cases corresponding to $\xi = 0^\circ$ and $\xi = 90^\circ$, one body is in the "shadow" of the other (see Appendix B), or a triple reflection is involved. For these reasons this consideration of multiple reflections is restricted to aspects in the range $15^\circ \leq \xi \leq 75^\circ$.

With this restriction we see from Equation A.6-1 that

$$\sigma_d < \frac{2\pi \rho_{11} \rho_{12} \rho_{21} \rho_{22}}{R^2} . \qquad (A.6\text{-}2)$$

This inequality indicates that it is not necessary to consider pairs of B-57 components having radii of curvature which are small with respect to R. It can be observed by examination of the B-57 drawings (Figures 1-1a, 1-1b, and 1-1c)

that many pairs of components can be immediately disregarded because the geometry is such that their normals are never perpendicular to one another. Therefore only the following are considered:

(1) the fuselage-engine combination,

(2) the fuselage-inner wing combination, and

(3) the "far" wing tank-"far" outer wing combination.

The fuselage-engine combination

This analysis is broken up into four parts depending on aspect. The first deals with aspects involving the front torus approximation for the engine, the second involves the front ogive approximation used for the engine, the third involves the rear ogive approximation for the engine, and the fourth deals with the remaining aspects.

It is readily seen from Equation A.6-1 that the "flatter" the surfaces are in the vicinity of the specular points, the larger will be the double-reflection contribution. Thus for the first category of aspects (i.e., $\cos\beta \cos\gamma > \cos\theta_o$, with $\theta_o = 55^o$), we find that the contribution of the fuselage-engine combination is always less than the contribution computed by Equation A.6-1 with $\rho_{11} = 1.00$m, $\rho_{12} = 40.3$m, $\rho_{21} = \rho_{22} = 0.39$m, and R = 2m. It is found that this upper bound is always less than the $\sum_{i=1}^{12} \sigma_i$ computed by the methods of the preceding sections of this appendix by a factor of at least three, and thus the double reflection contribution can be considered negligible within the accuracy of the aircraft cross-section computational procedure used here for this aircraft and for the aspects under discussion.

The contribution for the second category of aspects has been computed for aspects given approximately by $\gamma = 90^\circ - \epsilon$. (Here $\xi = 15^\circ$ corresponds to $\beta \approx 30^\circ$; $\xi = 55^\circ$ corresponds to $\beta \approx 68^\circ$; and $\xi \approx 67^\circ$ corresponds to $\beta \approx 120^\circ$. The $\xi \approx 15^\circ$ and $\xi \approx 67^\circ$ values represent the geometric limitations for double-reflections.) The contribution to the cross-section for these aspects is estimated using Equation A.6-1 with $\rho_{11} = 40.3$m, $\rho_{12} = 1.00$m, $\rho_{21} = 1.71$m, $\rho_{22} = 0.60$m, and R≈2m. Computation of this estimate shows that its magnitude is less by factors of thirty or more than the sum of the single-reflection contributions and thus can be neglected.

The third category of aspects is treated exactly as is the second except that the aspects are of the form $\gamma = 90^\circ + \epsilon$, and $\rho_{11} = 64.8$m, and $\rho_{21} = 4.82$m. The magnitude of this contribution (computed using Eq. A.6-1) is always less by at least a factor of ten than the corresponding $\sum_{i=1}^{12} \sigma_i$. Thus again the contribution can be neglected.

Aspects involving the rear of the engine would also involve the small prolate spheroid tail of the fuselage. The magnitude of the radii of curvature is sufficiently small and the values of R involved are sufficiently large to permit the conclusion that the contribution here is negligible on the basis of Equation A.6-2.

As can be seen from Sections A.2 and A.4, the central portions of the fuselage and engine are approximated by cylinders. The single-reflection cross-section of a cylinder varies (for normal aspects) as $1/\lambda$, and thus geometric optics ($\lambda \longrightarrow 0$) predicts an infinite cross-section for the cylinder at these aspects. Thus, physical optics rather than geometric optics would be required to obtain a meaningful estimate of the cross-section contribution

stemming from double-reflections from the two parallel cylinders. (This occurs only for $\gamma = 90^\circ$ and $\beta > 30^\circ$.) However, since it has been established that the double-reflection contribution is negligible (both for $\gamma = 90^\circ - \epsilon$ and $\gamma = 90^\circ + \epsilon$) and since continuity in the ratio of single-reflection contribution to double-reflection contribution is to be expected, it follows that the double-reflection contribution from the two cylinders at this aspect will be negligible in comparison to the sum of the single reflections. Thus, the actual determination of the magnitude of the double-reflection contribution by physical optics is not required.

In summary, the double-reflection contribution of the fuselage-engine combination is always negligible. From this it readily follows that the double-reflection contributions from such combinations as the fuselage and the wing tank or the engine and the wing tank are also negligible due to the smaller ρ_{ij} and the larger values of R.

The fuselage-inner wing combination

For $\beta \neq 0^\circ$ the breakup of the aircraft given in the earlier portions of this appendix indicates that a double-reflection contribution from the combination of the fuselage and the inner-wing surfaces is impossible since the normals to the bodies would never be perpendicular to each other. For $\beta = 0^\circ$, examination of the aircraft drawing indicates that double-reflections will occur for this combination. Study of the aircraft drawings indicates that although the breakup of the fuselage given in Section A.2 is adequate for single reflections (due to shadowing effects), the breakup must be modified for the double-reflection estimate. That is, in the $\beta = 0^\circ$ plane the fuselage is spheroidal in shape at the join of the fuselage and the inner wing with the

normals perpendicular at this join. An estimate of the magnitude of the double reflection contribution stemming from this combination for $\beta = 0^\circ$ can be obtained from a modified form of Equation A.6-1. Equation A.6-1 can be written in the form

$$\sigma_d = \frac{\pi \rho_{11} \rho_{12} \rho_{21}}{\sin(2\xi)\left[R\sin(2\xi) + \rho_{21}\cos\xi + \rho_{11}\sin\xi\right]\left[2\frac{R}{\rho_{22}} + \frac{\rho_{12}}{\rho_{22}}\cos\xi + \sin\xi\right]},$$

from which it follows that

$$\sigma_{d'} = \lim_{\substack{R\to 0 \\ \rho_{22}\to\infty}} \sigma_d = \frac{\pi \rho_{11}\rho_{12}\rho_{21}}{\sin(2\xi)\sin\xi\left[\rho_{21}\cos\xi + \rho_{11}\sin\xi\right]}.$$

Using $\sigma_{d'}$ to estimate this double reflection contribution, we have $\xi \approx 90^\circ - \gamma$, $\rho_{11} = 1.00$m, $\rho_{12} \approx 40.3$m, and $\rho_{21} = 0.052$m. This contribution is not negligible in comparison with the sum of the single-reflection contributions and thus is added to $\sum_{i=1}^{12} \sigma_i$ in obtaining the cross-section of the B-57 in the interval $0 < \gamma < 55^\circ$ for $\beta = 0^\circ$.

The far wing tank-far outer wing combination

The double-reflection contribution stemming from the combination of the far wing tank and the far outer wing will be relatively large only in the aspect range $\beta > 15^\circ$, $80^\circ < \gamma < 110^\circ$. An estimate of the magnitude of this contribution for $\gamma = 90^\circ$ (aspects for which the contribution will be a maximum) is obtained by using the limiting form of Equation A.6-1 when $\rho_{22} \to \infty$.

Here we have $\xi \approx \beta$, and $\rho_{11} = 4.29\text{m}, \rho_{12} = 0.4\text{m}, \rho_{21} = 9.65\text{m}$, with $R = (0.4\csc\xi)\text{m}$. This leads to estimates of the double-reflection contribution to the cross-section which are less by at least a factor of ten than the sum of the single-reflection contributions for these aspects. Thus this contribution can be considered to be negligible.

APPENDIX B

COMBINATION OF COMPONENT CROSS-SECTIONS

B.1 INTRODUCTION

As pointed out in Appendix A, the determination of the theoretical cross-section of an aircraft is broken down into three steps: considering the aircraft to be approximated by combinations of simple shapes (mathematically speaking), using approximation techniques to determine the cross-section contribution of these simple shapes (physical and geometric optics), and combining these component cross-sections in an appropriate manner to yield the cross-section of the aircraft itself.

Appendix A contains a complete discussion of the simple shapes used to approximate the parts of the aircraft and a listing of the formulas (taken from References 1 and 2) used to compute the cross-section contributions of each of these component parts. Appendix B is devoted to the third step, the procedure of combining these component cross-sections. The discussion is divided into two parts, one devoted to shadowing effects and the other to the actual combination of the component cross-sections.

B.2 SHADOWING EFFECTS

As pointed out in Reference 1, the cross-section of a partially shadowed component is unchanged unless the part of the body which contributes to the cross-section - that is, the part of the body which the incident radiation hits at normal incidence - is shadowed. In that case, since the specularly reflecting part of the body is shadowed, the component contributes only a negligible amount

to the cross-section. In what follows relative to the computation of the B-57 cross-sections, the term "shadowed" is applied to surfaces which are "inside" the aircraft as well as those which are shadowed in the usual sense.

A study of drawings of the B-57 led to the following conclusions relative to shadowing effects (for $-15^\circ \leq \beta \leq 90^\circ$ and $0^\circ \leq \gamma \leq 180^\circ$):

1. The fuselage, σ_1, is in shadow for $-15^\circ \leq \beta \leq 15^\circ$ at $\gamma = 90^\circ$ and for $85^\circ < \gamma < 90^\circ$ at $\beta = 0^\circ$.
2. The left wing tank, σ_2, is never in shadow for $-15^\circ \leq \beta \leq 90^\circ$.
3. The left engine, σ_3, is in shadow for $-15^\circ \leq \beta \leq 45^\circ$ at $\gamma = 90^\circ$.
4. The left inner wing, σ_4, the left outer wing, σ_5, and the left stabilizer, σ_6, contribute appreciable amounts to the cross-section only at very special aspects and shadowing never takes place at those aspects over the range of β involved in the computations.
5. The rudder surface, σ_7, is in shadow for many values of the azimuth angle for values of $\beta \geq 0^\circ$; however, because of the nature of the rudder surface, its contribution is negligible at these aspects and thus detailed information on shadowing is not required.
6. The right wing tank σ_8, is in shadow for $77^\circ \leq \beta \leq 110^\circ$ at $\gamma = -15^\circ$ and for $55^\circ < \gamma < 180^\circ$ at $\beta = 0^\circ$.
7. The right engine, σ_9, is in shadow for $-15^\circ \leq \beta \leq 45^\circ$ at $\gamma = 90^\circ$ and for $30^\circ \leq \gamma \leq 160^\circ$ at $\beta = 0^\circ$.
8. The right inner wing, σ_{10}, has a non-negligible contribution only in the vicinity of $\gamma = 0^\circ, \beta = 0^\circ$. Thus detailed information on shadowing effects is not required.

9. The right outer wing, σ_{11}, and the right stabilizer, σ_{12}, yield contributions which are always negligible. Thus no analysis of shadowing effects was performed.

Shadowing was taken into consideration in obtaining the value of σ_{13} (multiple scattering); this is discussed in Section A.6.

Thus, in determining the contribution of a given component to the cross-section of the aircraft at a given aspect, the value of the component cross-section is computed according to the formulas given in Appendix A and these values are used unless the component is in shadow. In that case the contribution of the component is taken to be negligible.

When a simple shape is partially in shadow, the contribution which arises from the shadow boundary is included. However, since the surface currents at such a boundary are continuous, fictitious sharp boundary effects must be omitted.

B.3 SUMMING THE COMPONENT CROSS-SECTIONS

In combining the values of the cross-sections of the component parts of the aircraft, it is assumed that the fields, when one averages the phase contributions of all the parts, are such that these contributions can be added in random phase.

This assumption is a valid one for the small wavelengths with which we are dealing here because the phase differences depend critically on aspect and on the dimensions of the aircraft. Since in practice the aspect is changing continually and the production dimensions of the aircraft vary enough to seriously affect phase relations, averaging is the most meaningful procedure.

This leads to the simple addition of the radar cross-sections of the various parts of the body in finding the cross-section of the composite body itself. An upper bound on the maximum error involved can be computed from Formula A.1-6 in Reference 1; at X- and S-bands, however, such a calculation is not necessary.

Thus, the cross-section of the B-57, $\sigma(\beta, \gamma)$, is obtained by the relation

$$\sigma(\beta, \gamma) = \sum_{i=1}^{13} \sigma_i(\beta, \gamma) \quad ,$$

where the σ_i are as defined in Appendix A. If shadowing effects take place the value of the σ_i involved is replaced by zero.

In connection with the step of combining these component cross-sections one additional item is worthy of consideration here. That item involves the question of the width of sharp peaks, such as those obtained at particular aspects for such shapes as cylinders, truncated cones, the torus, and tapered wedges. The physical optics methods employed to derive the formulas for these contributions yield one expression for "normal" incidence and a second expression for "non-normal" incidence. At short wavelengths the contribution at normal incidence is considerably larger than at non-normal incidence. If the body is sharply terminated, the widths of the peaks can be measured by using the relationships given in Section A.1.7 of Reference 1 and extensions of these relations. If, on the other hand, the ends of the body are not sharply terminated but instead are smoothly rounded, the result is a "pencil sharp" peak. For the purpose of the presentation of the B-47 data in

Section II, bounds to the width of these peaks are shown; that is, for the purpose of obtaining an upper bound to the width of the peaks, it is assumed that the contributor involved is sharply terminated. Thus the bounding peak widths are determined from the relations given in Reference 1 and the extensions of those relations.

REFERENCES

1. C. E. Schensted, J. W. Crispin, and K. M. Siegel, "Studies in Radar Cross-Sections XV - Radar Cross-Sections of B-47 and B-52 Aircraft", The University of Michigan, Engineering Research Institute, Report No. 2260-1-T, August 1954. CONFIDENTIAL

2. R. R. Bonkowski, C. R. Lubitz, and C. E. Schensted, "Studies in Radar Cross-Sections VI - Cross-Sections of Corner Reflectors and Other Multiple Scatterers at Microwave Frequencies", The University of Michigan, Engineering Research Institute, Report No. UMM-106, October 1953. SECRET (UNCLASSIFIED when Appendix is removed).

3. S. Ratcliffe, "Aircraft Echoes at X-Band (1)", Telecommunications Research Establishment, Gt. Malvern, Worcs., England, Memorandum 750 (June 1953). CONFIDENTIAL.